BIOMATERIALS

An off-the-shelf bioadhesive patch for sutureless repair of gastrointestinal defects

Jingjing Wu[1]†, Hyunwoo Yuk[1]†*, Tiffany L. Sarrafian[2]†, Chuan Fei Guo[3], Leigh G. Griffiths[4]*, Christoph S. Nabzdyk[5]*, Xuanhe Zhao[1,6]*

Surgical sealing and repair of injured and resected gastrointestinal (GI) organs are critical requirements for successful treatment and tissue healing. Despite being the standard of care, hand-sewn closure of GI defects using sutures faces limitations and challenges. In this work, we introduce an off-the-shelf bioadhesive GI patch capable of atraumatic, rapid, robust, and sutureless repair of GI defects. The GI patch integrates a nonadhesive top layer and a dry, bioadhesive bottom layer, resulting in a thin, flexible, transparent, and ready-to-use patch with tissue-matching mechanical properties. The rapid, robust, and sutureless sealing capability of the GI patch is systematically characterized using ex vivo porcine GI organ models. In vitro and in vivo rat models are used to evaluate the biocompatibility and degradability of the GI patch in comparison to commercially available tissue adhesives (Coseal and Histoacryl). To validate the GI patch's efficacy, we demonstrate successful sutureless in vivo sealing and healing of GI defects in rat colon, stomach, and small intestine as well as in porcine colon injury models. The proposed GI patch provides a promising alternative to suture for repair of GI defects and offers potential clinical opportunities for the repair of other organs.

INTRODUCTION

Failure of surgical repair of gastrointestinal (GI) defects can lead to anastomotic leaks, one of the most feared and life-threatening complications after GI surgeries, resulting in more than 30% increase in mortality (*1*, *2*). Surgical sealing and repair of GI defects are commonly achieved by hand-sewn closure of GI tissues using sutures. However, despite being the standard of care, GI organ sealing through sutures remains associated with a high rate of anastomotic leaks (i.e., up to 20% in high-risk patients), resulting in serious complications, including infection, sepsis, and even death (*1*–*5*). Failure to seal surgically repaired GI tissues can be due to various factors (*1*, *6*), including the inherent disadvantages of suture-based tissue sealing: (i) complicated technical processes that require high surgical skill, (ii) tissue damage due to needle piercing, and (iii) pointwise closure leading to stress concentration around the sutured points (*2*, *3*, *5*, *7*, *8*). As an alternative to sutures, surgical staplers have been increasingly adopted for GI surgeries. However, surgical staplers also impose similar limitations of tissue damage, pointwise closure, and stress concentration, and they do not substantially reduce the rate of leaks compared with sutures (*9*). Hence, surgical repair of GI defects to provide mechanical sealing and favorable healing still remains an ongoing challenge, highlighting the critical importance of developing new treatments and solutions.

Tissue adhesives and sealants have recently emerged as a potentially advantageous alternative or adjunct to sutures or staples in various clinical indications (*7*, *8*, *10*–*17*). However, existing tissue adhesives and sealants are commonly deployed in the form of viscous liquids, and they usually require a diffusion-based interpenetration into tissues (*11*, *13*, *14*) and/or solidification by chemical reaction or external stimuli such as ultraviolet (UV) light (*13*–*15*) to form tissue sealing. As another example, in situ application of polymer fibers has also been used as tissue sealants based on blow spinning of adhesive precursor solutions (*18*–*20*). These features of existing tissue adhesives and sealants result in several limitations, including slow and/or weak tissue sealing, the need for external devices (e.g., UV source, fluidic mixer, and pressurized air-based blow spinner), and/or complicated preparations and applications (e.g., thawing, mixing, or light irradiation) (*13*, *14*, *19*, *21*), which render them insufficient for facile and robust repair of GI defects. More recently, to overcome the limitations of existing technologies, several bioadhesives have been developed to provide rapid and/or tough adhesion to wet tissues (*20*, *22*–*26*). However, the materials used and their underlying sealing mechanisms have not been sufficiently optimized for challenging clinical applications such as the repair of GI defects.

In this study, we introduce an off-the-shelf bioadhesive patch platform, named GI patch, as a therapeutic solution for the treatment of GI defects. Inspired by the convenience and effectiveness of duct tape in nonmedical applications, the GI patch offers facile, atraumatic, fluid-tight, robust, and sutureless sealing of GI defects while addressing key limitations of sutures and commercially available tissue adhesives and sealants (Fig. 1, A and B). We systematically characterized the GI tissue–matching mechanical properties and superior adhesion of the GI patch as compared with commercially available tissue adhesives (Histoacryl, Coseal, and Tisseel) using ex vivo porcine models. The biocompatibility and degradability of the GI patch were thoroughly validated through in vitro cytotoxicity evaluation in human intestinal epithelial cells, and in vivo histopathology, immunofluorescence, quantitative polymerase chain reaction (qPCR), enzyme-linked immunosorbent assay (ELISA), and blood analyses in rat models. We further validated the in vivo efficacy of sutureless repair of GI defects by the GI patch in rat colon, stomach, and small intestine injury models as well as a porcine colon injury model.

[1]Department of Mechanical Engineering, Massachusetts Institute of Technology, Cambridge, MA 02139, USA. [2]Department of Thoracic Surgery, Mayo Clinic, Rochester, MN 55905, USA. [3]Department of Materials Science and Engineering, Southern University of Science and Technology, Shenzhen 518055, China. [4]Department of Cardiovascular Medicine, Mayo Clinic, Rochester, MN 55905, USA. [5]Department of Anesthesiology and Perioperative Medicine, Mayo Clinic, Rochester, MN 55905, USA. [6]Department of Civil and Environmental Engineering, Massachusetts Institute of Technology, Cambridge, MA 02139, USA.
*Corresponding author. Email: hyunwoo@mit.edu (H.Y.); griffiths.leigh@mayo.edu (L.G.G.); nabzdyk.christoph@mayo.edu (C.S.N.); zhaox@mit.edu (X.Z.)
†These authors contributed equally to this work.

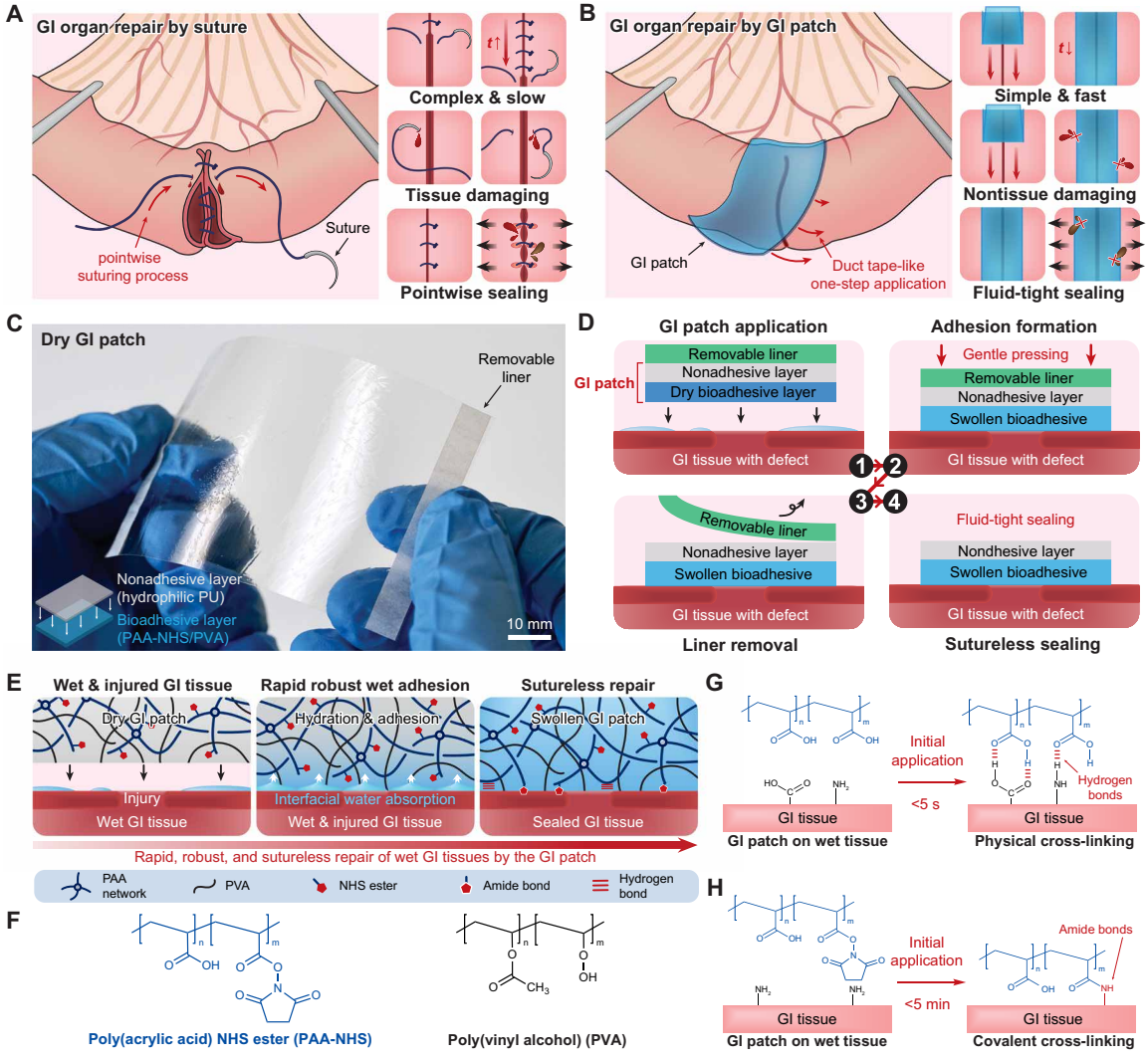

Fig. 1. Design and mechanism of sutureless repair by the GI patch. (**A**) Schematic illustrations for repair of GI defects by sutures. (**B**) Schematic illustrations for sutureless repair of GI defects by the GI patch. (**C**) Photograph of the dry GI patch and a schematic illustration (bottom left) for its structure consisting of the nonadhesive top layer based on hydrophilic PU and the bioadhesive bottom layer based on PAA-NHS and PVA. (**D**) Schematic illustrations for the components of the GI patch and for the stepwise processes of sutureless repair of GI defects by the GI patch. (**E**) Schematic illustrations for mechanism of sutureless repair of GI defects by the GI patch based on the dry cross-linking process. (**F**) Chemical composition of the GI patch based on PAA-NHS and PVA. (**G** and **H**) Schematic illustrations for rapid wet adhesion of the GI patch to the GI tissue surface by physical cross-linking based on hydrogen bonds (G) and covalent cross-linking based on amide bonds (H). Scale bars, 10 mm (C).

RESULTS

Design and mechanisms of the GI patch

The GI patch is a thin, flexible, and transparent dressing consisting of a nonadhesive top layer and a dry, bioadhesive bottom layer (Fig. 1C and fig. S1). A removable liner layer can be further assembled on top of the nonadhesive layer to improve the handling of the GI patch in certain applications (Fig. 1, C and D). The nonadhesive top layer consists of hydrophilic polyurethane (PU), which acts as a nonadhesive interface to the surrounding tissues while providing tissue-matching and robust mechanical properties to the GI patch. The dry, bioadhesive bottom layer consists of interpenetrating networks between the covalently cross-linked poly(acrylic acid) *N*-hydroxysuccinimide (NHS) ester (PAA-NHS) for bioadhesiveness and the physically cross-linked poly(vinyl alcohol) (PVA) for mechanical reinforcement (Fig. 1, E and F, and fig. S2). The bioadhesive can quickly and robustly adhere to wet GI tissues based on a dry cross-linking mechanism (*23*, *24*, *27*). In brief, the hydrophilic and hygroscopic PAA-NHS and PVA in the dry bioadhesive layer allow the absorption and drying of interfacial water on wet GI tissues upon contact (Fig. 1E) (*23*, *27*). Subsequently, the carboxylic acid groups and NHS ester groups in the PAA-NHS network facilitate rapid and robust adhesion to the GI tissue surface based on physical cross-linking via hydrogen bonds (Fig. 1G) and covalent cross-linking via amide bonds (Fig. 1H), respectively (*23*, *24*, *28*). The off-the-shelf flexible dressing form factor and the facile adhesion to wet GI tissues without the need of other devices or stimuli (e.g., UV and blow spinner) endow the GI patch with ready-to-use features, similar to those features of duct tapes.

After adhering to GI tissues and sealing GI defects, the GI patch was further hydrated and swelled in a wet physiological environment (figs. S3 and S4) into a soft (Young's modulus of 135 kPa), stretchable

(more than five times of the original length; fig. S5A), and robust (fracture toughness of 758 J m^{-2}; fig. S6) hydrogel. The swelling-driven lateral dimensional changes (i.e., increase in length and width) of the GI patch have been eliminated (fig. S3) by introducing a pre-stretch to the dry bioadhesive layer equivalent to its equilibrium swelling ratio during the GI patch preparation (fig. S1) (*29*). This unique characteristic of the GI patch prevents separation of approximated wound edges and subsequent delayed healing, which is a common problem encountered when using swellable tissue adhesives and sealants (*8*). To minimize the GI patch's mechanical mismatch with GI tissues, the Young's modulus of the GI patch was optimized to match that of ex vivo porcine colon and stomach (fig. S5, B to D). Furthermore, the GI patch maintains consistent mechanical properties in terms of Young's modulus, ultimate tensile stretch, and tensile strength up to 1 month in physiological environments (fig. S7), suggesting that it could offer mechanical stability and integrity during critical stages of GI tissue defect healing.

Adhesive performance

To quantitatively evaluate the adhesive properties of the GI patch, we characterized interfacial toughness, shear strength, tensile strength, and burst strength when applied to wet porcine colon and stomach tissues ex vivo (Fig. 2 and fig. S8). The GI patch adhered to GI tissues upon contact for 5 s, with high interfacial toughness (>480 J m^{-2} for colon; >560 J m^{-2} for stomach), shear strength (>80 kPa for colon; >90 kPa for stomach), and tensile strength (>75 kPa for colon; >85 kPa for stomach) measured 5 min after application (Fig. 2, A to F). The adhesive performance of the GI patch slightly decreased when the GI patch was in the fully swollen state (measured 6 hours after the initial application) (fig. S4, D to G), because of the decreased mechanical properties of the GI patch as its water contents increase until reaching the fully swollen state (fig. S4, A to C); however, the decreased adhesive properties were not statistically significant except for burst pressure (fig. S4G). Nonetheless, the fully swollen GI patch exhibited superior adhesive performance with high interfacial toughness (>350 J m^{-2} for colon; >500 J m^{-2} for stomach), shear strength (>65 kPa for colon; >80 kPa for stomach), and tensile strength (>60 kPa for colon; >65 kPa for stomach) in comparison with commercially available tissue adhesives and sealants, including cyanoacrylate glue (Histoacryl), poly(ethylene glycol) (PEG)–based sealant (Coseal), and fibrin glue (Tisseel) measured per the manufacturer's guidelines (1 min after application for Histoacryl, 3 min for Coseal, and 3 min for Tisseel) for both porcine colon and stomach (Fig. 2, A to F; fig. S4, D to G; and data files S1 and S2).

We further evaluated sutureless fluid-tight sealing of GI defects by applying the GI patch to wet porcine colon and stomach tissues

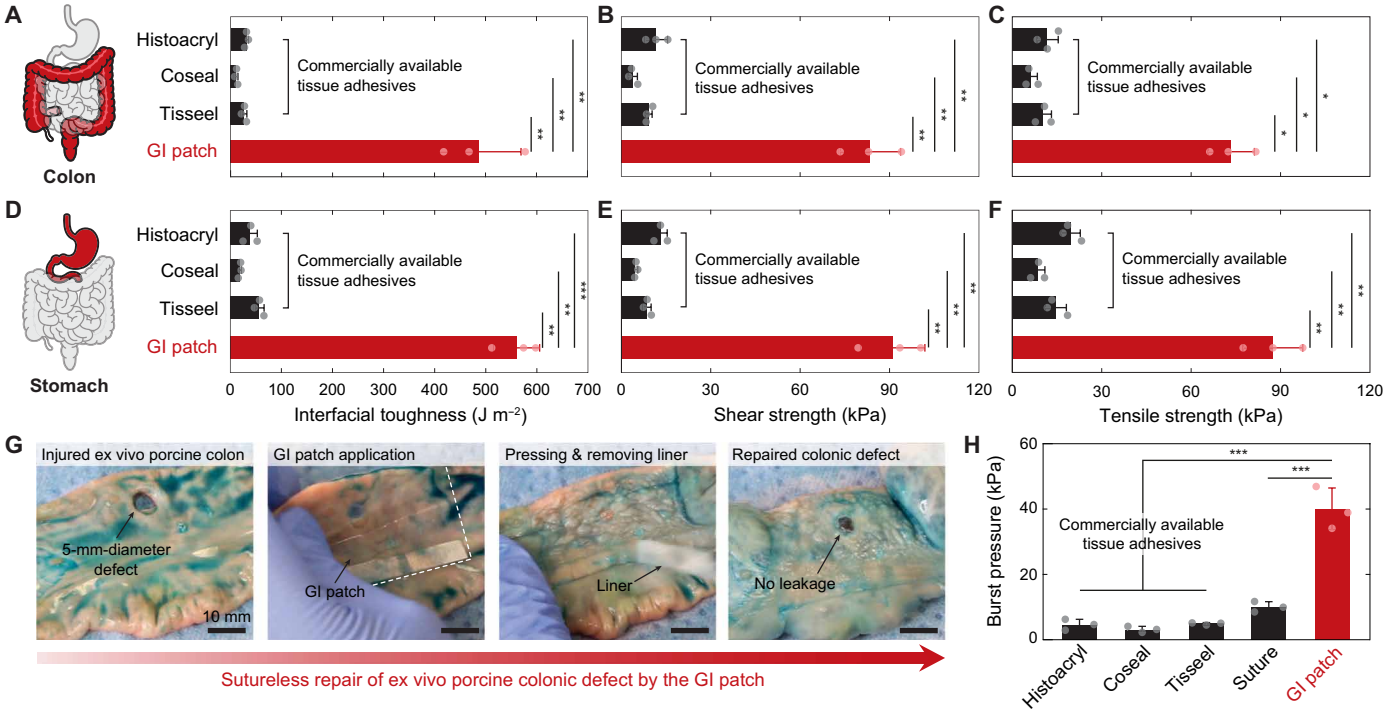

Fig. 2. Adhesion performance of the GI patch. (**A** to **C**) Adhesion performance of the GI patch and the commercially available tissue adhesives for interfacial toughness (A), shear strength (B), and tensile strength (C) on ex vivo porcine colon. (**D** to **F**) Adhesion performance of the GI patch and the commercially available tissue adhesives for interfacial toughness (D), shear strength (E), and tensile strength (F) on ex vivo porcine stomach. (**G**) Snapshots of rapid and robust sutureless repair of 5-mm-diameter defects in an ex vivo porcine colon by the GI patch. Saline applied to the porcine colon was colored with blue dye for visual. (**H**) Burst pressure of ex vivo porcine colons with a 5-mm-diameter defect sealed by the GI patch, the commercially available tissue adhesives, and sutures. The porcine colon and stomach were covered with saline before application of the GI patch or commercially available tissue adhesives to ensure wetness of tissues. The adhesion performance of the GI patch and commercially available tissue adhesives was tested 5 min after the initial application; commercially available adhesives were applied per the manufacturer's guidelines (measured after 1 min of application for Histoacryl, 3 min for Coseal, and 3 min for Tisseel). Values in (A) to (F) and (H) represent the means ± SD ($n = 3$). *P* values are determined by two-sided *t* test for the comparisons between two groups and by one-way ANOVA followed by the Bonferroni's multiple comparison test for the comparison between multiple groups; $^{*}P < 0.05$; $^{**}P \leq 0.01$; $^{***}P \leq 0.001$. Scale bars, 10 mm (G).

ex vivo (Fig. 2G). The GI patch readily formed fluid-tight sealing of 5-mm-diameter defects in porcine colon (movie S1) and stomach (movie S2) within 10 s of application. Moreover, the seal formed by the GI patch exhibited high burst pressure of >24 kPa for the fully swollen GI patch and >40 kPa for the patch applied for 5 min, outperforming the commercially available tissue adhesives and sealants as well as sutures (Fig. 2H, fig. S4G, and data files S1 and S2).

Biocompatibility and degradability

To quantitatively evaluate the biocompatibility and degradability of the GI patch, we performed in vitro and in vivo tests. In vitro LIVE/DEAD staining of human intestinal epithelial cells (Caco-2) cultured in GI patch–incubated media for 24 hours showed comparable cell viability to the control media group ($P = 0.12$), whereas exposure to cell media incubated with the commercially available tissue adhesives (Coseal and Histoacryl) resulted in significantly lowered cell viability compared with the control media group (Fig. 3A and data file S3). In vivo biocompatibility of the GI patch and the commercially available tissue adhesives (Coseal and Histoacryl) was assessed by implantation onto intact rat colon and stomach for 4 weeks (fig. S9), followed by histopathology, immunofluorescence, qPCR, and ELISA analyses (Fig. 3, B to I, and figs. S10 and S11). The histological evaluation by a blinded pathologist indicated that the GI patch induced minimal to no inflammation to the underlying and surrounding GI tissues (Fig. 3F and fig. S10C), comparable to that of the Coseal group (Fig. 3B and fig. S10A). In contrast, cyanoacrylate glue (Histoacryl) exhibited lower in vivo biocompatibility than the GI patch and Coseal groups, with observations of mild inflammation and fibrosis (Fig. 3D and fig. S10B), in agreement with a previous report (*25*). The Histoacryl group showed marked fibrotic adhesion to the surrounding tissues (fig. S9, B and E), whereas such macroscopic fibrotic adhesions were not observed in the GI patch and Coseal groups.

We further evaluated in vivo biocompatibility of the GI patch using immunofluorescence staining (Fig. 3, C, E, and G) and normalized immunofluorescence intensity analysis (Fig. 3H and data file S3) of fibroblasts [alpha smooth muscle actin (aSMA) and collagen III], macrophages [CD68 for pan-macrophage, inducible nitric oxide synthase (iNOS) and vimentin for M1 type, and CD206 for M2 type], T cells (CD3), and fibrosis (collagen I). The GI patch induced comparable inflammatory and foreign body response to the Coseal group, whereas the Histoacryl group showed significantly greater inflammatory and foreign body responses than both groups (Fig. 3H). Relative gene expression for fibroblast (*Acta2* for aSMA and *Col3a1* for collagen III), M1 type macrophage (*Cd86* for CD86 and *Nos2* for iNOS), M2 type macrophage (*Mrc1* for CD206 and *Arg1*), T cell [*IL2* for interleukin-2 (IL-2)], and fibrosis (*Col1a1* for collagen I) markers via qPCR analysis also showed good agreement with the immunofluorescence analysis (Fig. 3I and data file S3). ELISA for inflammatory cytokines [IL-6 and tumor necrosis factor–α (TNF-α)] showed that the GI patch induced lower concentrations of IL-6 and TNF-α than both the Coseal and Histoacryl groups (fig. S11).

Next, we investigated in vivo degradability of the GI patch in a rat subcutaneous implantation model for up to 12 weeks (Fig. 4A). The hydrophilic PU was also implanted separately to better investigate its in vivo degradation characteristics as an individual material. Both hydrophilic PU (nonadhesive layer of the GI patch) and the GI patch exhibited a gradual decrease in size (Fig. 4, B and C, and fig. S12) and weight (Fig. 4D and data file S4) during the implantation period, with substantial degradation observed by 12 weeks after implantation. Histological evaluation of the implanted GI patch showed a similar trend with marked degradation and fragmentation of the GI patch at 12 weeks after implantation (Fig. 4E). The in vivo degradability of the GI patch originates from gradual hydrolytic degradation and dissolution of hydrophilic PU (nonadhesive layer) (*30*, *31*) and degradable cross-linkers [i.e., PEG dimethacrylate (PEGDMA)] in the bioadhesive layer (*32*). We further performed blood analyses, including complete blood counts (CBCs) and comprehensive blood chemistry panels, to evaluate potential systemic toxicity of degradation by-products. Throughout the study period up to 12 weeks, the blood analyses of animals with the implanted GI patch resulted in comparable results to that of healthy animals without marked sign of systemic toxicity (Fig. 4, F and G, and data file S4).

Sutureless repair and healing of GI defects in rat models

To validate the in vivo efficacy of sutureless repair of GI defects by the GI patch, we evaluated sealing and healing of rat colon and stomach defects by the GI patch in comparison with sutures as a standard care control (Fig. 5A and figs. S13 to S16). The GI patch can be prepared into a ready-to-use package either with or without a removable liner as a backing substrate (fig. S1B): To facilitate easier handling of the thin GI patch for applications in small animals, we used the GI patch with a removable liner when repairing GI defects in the rat models. Patch application provided atraumatic and fluid-tight sealing of 10-mm incisional defects in rat colon (Fig. 5B and movie S3) and stomach (fig. S13B and movie S4) in less than 10 s without further preparation steps or use of additional devices (e.g., mixer, UV light, and blow spinner). In contrast, the pointwise tissue closure by sutures took longer to perform (>2 min) and caused puncture-driven tissue damage (fig. S14). After 4 weeks, both groups (the GI patch and sutures) showed healing of the defects without macroscopic evidence of GI leaks. The GI patch maintained robust adhesion to the underlying GI tissues in all rats in the study as observed upon euthanasia (i.e., 4 weeks) (Fig. 4C and fig. S13C). There were more postsurgical adhesions to the surrounding organs observed in animals treated with sutures (four of eight animals for colon, and one of four animals for stomach) as compared with the animals treated with the GI patch (0 animal for both colon and stomach) 4 weeks after repair (fig. S17).

To evaluate efficacy of the GI patch over the course of the healing process, we performed histological, immunofluorescence, and qPCR analyses 1 and 4 weeks after repair of rat colon in comparison with the standard care group treated with sutures (Fig. 5, D to I, and fig. S15). The histological assessment by a blinded pathologist indicated that the defects repaired by either sutures or GI patch were in the acute healing process 1 week after repair (fig. S15, A to D). After 4 weeks, the defect repaired by the GI patch healed with a minimal fibrotic cyst formation only on the top of the GI patch (Fig. 5F and fig. S16D), whereas the sutured defect healed with mild inflammation and fibrosis around the sutures (Fig. 5D and fig. S16B).

Immunofluorescence staining (fig. S15, B and D) and normalized immunofluorescence intensity analysis (fig. S15E) of fibroblast (aSMA and collagen III), macrophage (CD68 for pan-macrophage, iNOS and vimentin for M1 type, and CD206 for M2 type), T cell (CD3), and fibrosis (collagen I) markers 1 week after repair showed elevated abundance of aSMA, collagen I, and collagen III in the GI patch group compared with the suture group (*33*, *34*). A similar trend of

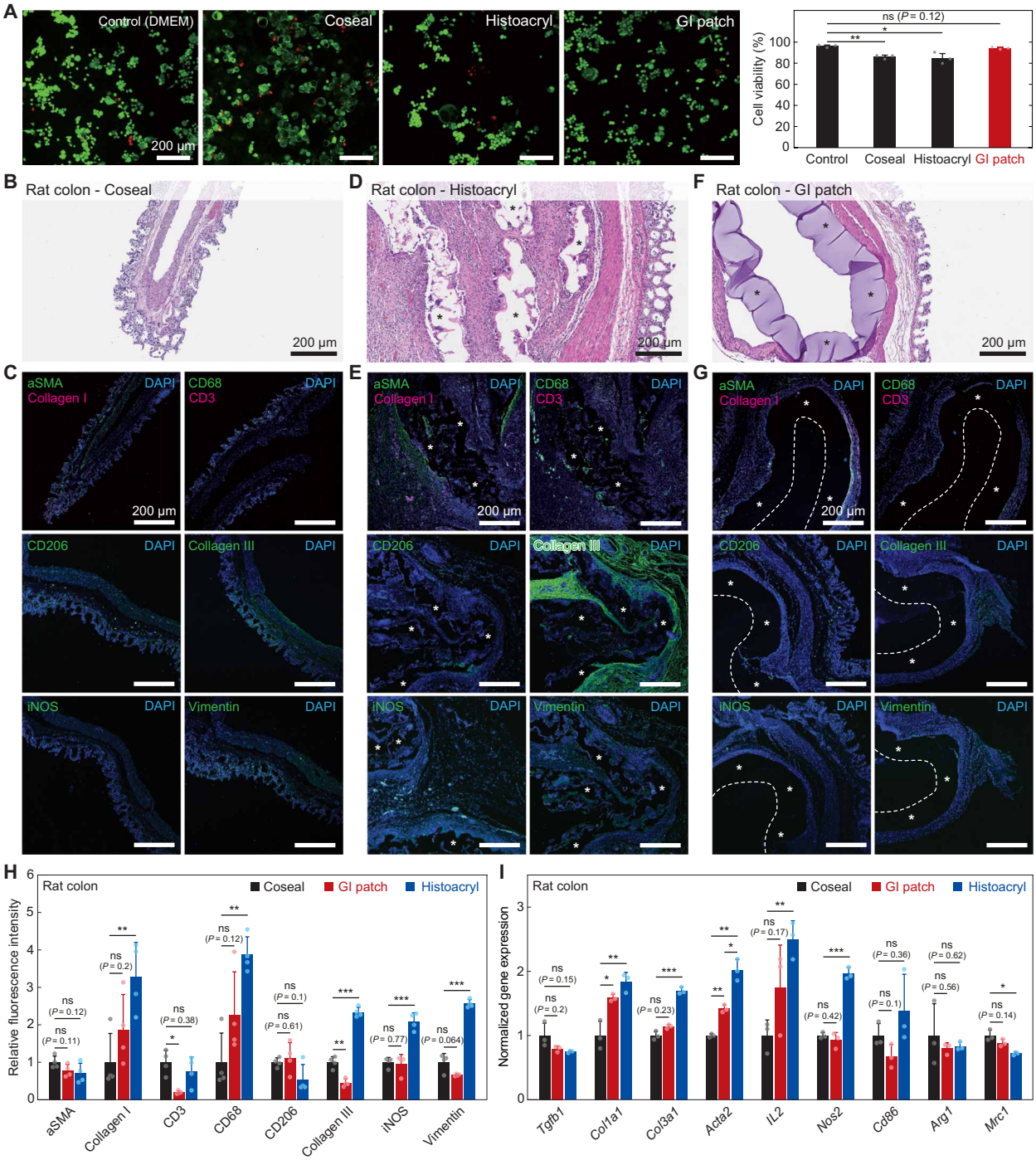

Fig. 3. In vitro and in vivo biocompatibility of the GI patch. (**A**) Representative LIVE/DEAD assay images (left) and the cell viability (right) of human intestinal epithelial cells (Caco-2) for control (DMEM), Coseal, Histoacryl, and the GI patch after 24-hour culture. DMEM, Dulbecco's modified Eagle's medium. (**B** to **G**) Representative histological images stained with H&E and immunofluorescence images for Coseal (B and C), Histoacryl (D and E), and the GI patch (F and G) at 4 weeks after implantation to rat colon. In histological images, * represents the implanted Histoacryl (D) and GI patch (F). In immunofluorescence images, blue fluorescence corresponds to cell nuclei stained with 4′,6-diamidino-2-phenylindole (DAPI); green fluorescence corresponds to the expression of fibroblasts (aSMA), collagen III, vimentin, pan macrophage (CD68), M1 type macrophage (iNOS), or M2 type macrophage (CD206) as indicated; red fluorescence corresponds to the expression of collagen I and T cells (CD3) as indicated; * represents the implanted Histoacryl (E) and GI patch (G); dotted line represents the edge of the implanted GI patch. (**H**) Normalized fluorescence intensity from the immunofluorescence images for aSMA, collagen I, collagen III, vimentin, CD3, CD68, iNOS, and CD206 at 4 weeks after implantation of Coseal, Histoacryl, and the GI patch to rat colon. (**I**) Normalized gene expression of inflammation-related markers in rat colon at 4 weeks after implantation of Coseal, Histoacryl, and the GI patch. Values in (A), (H), and (I) represent the means ± SD [$n = 3$ in (A) and (I); $n = 4$ in (H)]. P values are determined by two-sided t test; ns, not significant; $^*P < 0.05$; $^{**}P \leq 0.01$; $^{***}P \leq 0.001$. Scale bars, 200 μm (A to G).

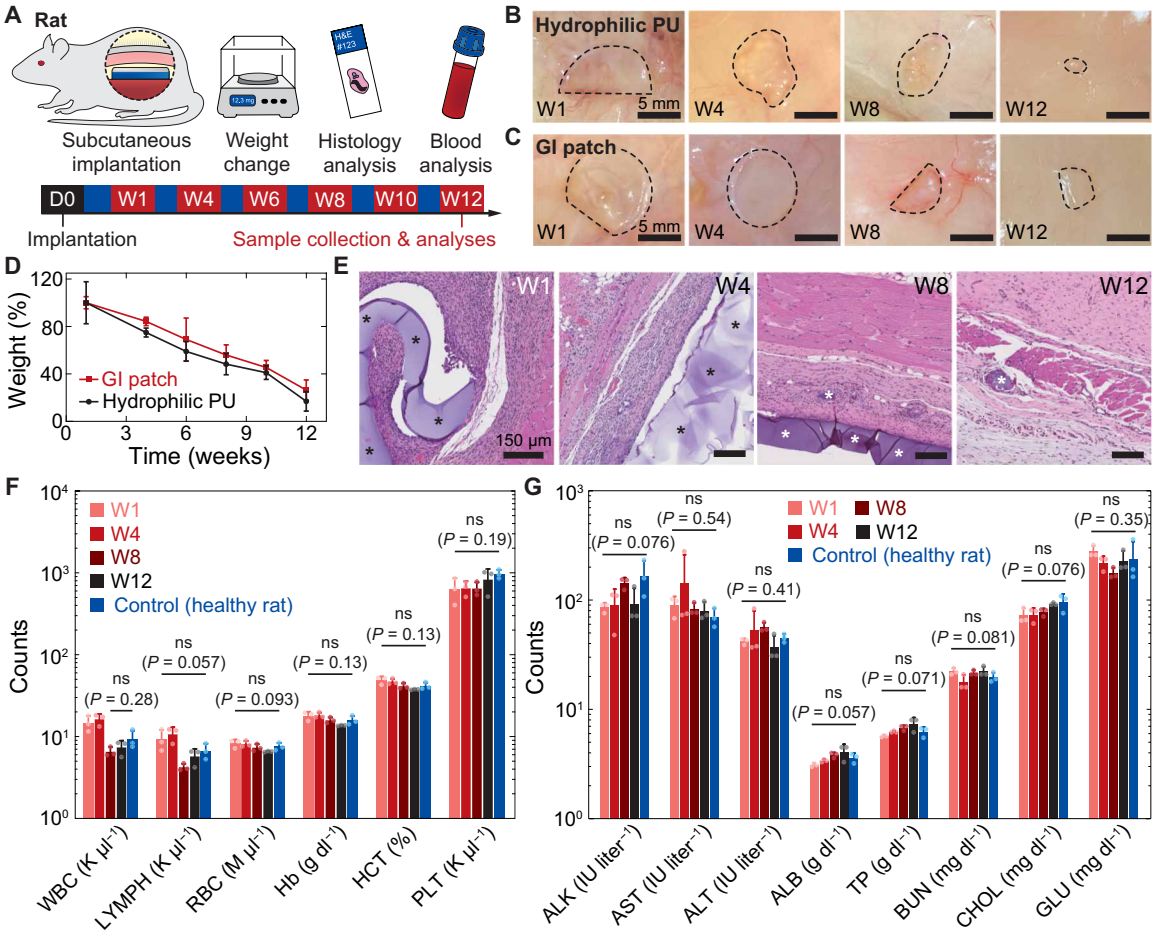

Fig. 4. In vivo degradation of the GI patch in rat subcutaneous model. (**A**) Schematic illustrations for in vivo degradation studies of the GI patch. D, day; W, week. (**B** and **C**) Images of the subcutaneously implanted hydrophilic PU (B) and GI patch (C) at 1, 4, 8, and 12 weeks after implantation. Dotted lines represent the edge of the implanted samples. (**D**) Remaining weight of the subcutaneously implanted GI patch and hydrophilic PU at various postimplantation durations. (**E**) Representative histological images stained with H&E for the subcutaneously implanted GI patch at 1, 4, 8, and 12 weeks after implantation. * represents the implanted GI patch. (**F**) Complete blood count (CBC) of control (healthy animal without surgery) and animals with the subcutaneously implanted GI patch at 1, 4, 8, and 12 weeks after implantation. WBC, white blood cell; LYMPH, lymphocyte; RBC, red blood cell; Hb, hemoglobin; HCT, hematocrit; PLT, platelet. (**G**) Blood chemistry of control (healthy animal without surgery) and animals with the subcutaneously implanted GI patch at 1, 4, 8, and 12 weeks after implantation. ALK, alkaline phosphatase; AST, aspartate transaminase; ALT, alanine transaminase; ALB, albumin; TP, total protein; BUN, blood urea nitrogen; CHOL, cholesterol; GLU, glucose. Values in (D), (F), and (G) represent the means ± SD ($n = 3$). *P* values are determined by one-way ANOVA followed by the Bonferroni's multiple comparison test; ns, not significant. Scale bars, 5 mm (B and C) and 150 μm (E).

elevated gene expression for *Acta2*, *Col1a1*, and *Col3a1* in the GI patch group was observed in the qPCR analysis (fig. S15F). After 4 weeks, immunofluorescence staining (Fig. 5, E and G) and normalized immunofluorescence intensity analysis (Fig. 5H and data file S5) showed significantly lower collagen I, collagen III, and M1 type macrophage markers (iNOS and vimentin) in the GI patch group compared with the suture group. A similar trend of lower gene expression for *Col1a1*, *Col3a1*, and M1 type macrophage (*Cd86* and *Nos2*) in the GI patch group was observed in the qPCR analysis (Fig. 5I and data file S5). This lower *Col1a1*, *Col3a1*, and M1 type macrophage expression in the GI patch group indicates a lower degree of fibrosis and inflammatory response in the GI patch group during the long-term healing process, in agreement with the fibrosis and inflammation observed in the histological evaluation of the suture group (Fig. 5D and fig. S16B).

In both GI patch– and suture-treated animals, other organs (kidney, liver, spleen, and lung) not directly treated by sutures or patches appeared to be normal, without indications of inflammation or damage caused by leaks from the GI defects (fig. S18). Blood analyses based on CBC (fig. S19A) and blood chemistry (fig. S19B) 4 weeks after repair did not show significant differences between the healthy rat control group and the GI defect repair groups, further confirming that both sutures and the GI patch can prevent anastomotic leaks without subsequent systemic inflammation during the healing of the GI defects (*35*).

In addition to sutureless repair of linear incisional defects by the GI patch in the rat colon and stomach models, we investigated sutureless anastomosis using the GI patch or sutured anastomosis as a standard care control in a rat small intestine model (fig. S20A). The circumferentially applied GI patch formed fluid-tight sutureless

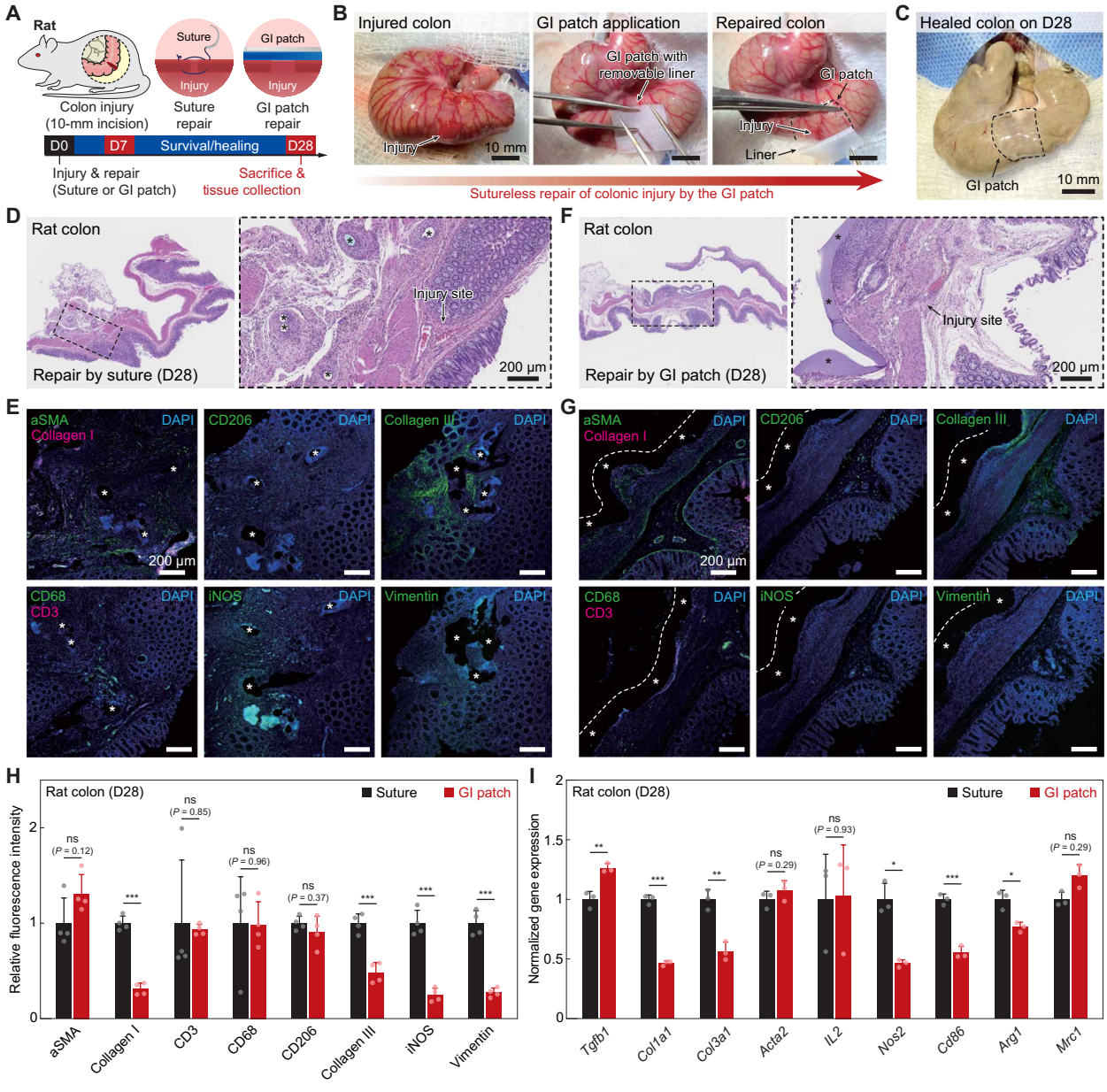

Fig. 5. Sutureless repair of GI defects in rat model. (**A** and **B**) Schematic illustrations (A) and experimental images (B) for in vivo defect-repair studies of rat colon by sutures and the GI patch. (**C**) Rat colon 28 days (D28) after sutureless repair by the GI patch. (**D** to **G**) Representative histological images stained with H&E and immunofluorescence images for rat colon defect repaired by sutures (D and E) and the GI patch (F and G) after 28 days. In histological images, * represents the sutures (D) and GI patch (F). In immunofluorescence images, blue fluorescence corresponds to cell nuclei stained with DAPI; green fluorescence corresponds to the expression of fibroblast (aSMA), collagen III, vimentin, pan macrophage (CD68), M1 type macrophage (iNOS), and M2 type of macrophage (CD206); red fluorescence corresponds to the expression of collagen I and T cell (CD3); * represents the sutures (E) and GI patch (G); dotted line represents the edge of the implanted GI patch. (**H**) Normalized fluorescence intensity from the immunofluorescence images for aSMA, collagen I, collagen III, vimentin, CD3, CD68, iNOS, and CD206 at 28 days after repair by sutures and the GI patch. (**I**) Normalized gene expression of inflammation-related markers in rat colon at 28 days after repair by sutures and the GI patch. Values in (H) and (I) represent the means ± SD [$n = 4$ in (H); $n = 3$ in (I)]. P values are determined by two-sided t test; ns, not significant; $^*P < 0.05$; $^{**}P \leq 0.01$; $^{***}P \leq 0.001$. Scale bars, 10 mm (B and C) and 200 μm (D to G).

anastomosis of a rat small intestine (~90% diameter cut) in less than 10 s (fig. S20B). After 4 weeks, anastomotic sites repaired by either sutures or GI patch exhibited healing of the defects without macroscopic sign of GI leaks (fig. S20, C and E). Histological assessment by a blinded pathologist indicated that the anastomotic site treated with the GI patch healed with mild inflammation and fibrosis, comparable to the sutured anastomosis (fig. S20, D and F).

Sutureless repair and healing of GI defects in porcine models

To further validate in vivo efficacy and to demonstrate the scalability of the technology, we used GI patches to seal two adjacent 5-mm-diameter porcine colonic defects per pig (Fig. 6, A and B). In total, five pigs received a combined ten 5-mm-diameter colon injuries. We tested the GI patch with and without removable liner (fig. S1B) in the in vivo porcine colonic defect-repair model to assess

user-friendliness and treatment efficacy of different packaging methods for the GI patch (Fig. 6C).

GI patches with and without removable liners provided fluid-tight sealing of porcine colonic defects in less than 10 s (Fig. 6D and movie S5), offering rapid and robust sutureless repair of GI defects. The GI patch without removable liner exhibited more favorable haptic feedback for the operating surgeons in terms of conformal adhesion to GI defects, owing to the unimpeded optical transparency of the package compared with the GI patch with removable liner. All pigs survived repair of a total of 10 potentially lethal colonic defects (two adjacent 5-mm punch holes per pig) by the GI patch and displayed normal feeding behavior with associated weight gain. There were no signs of abnormal health conditions (e.g., fever or lethargy) or complications associated with wound healing based on daily veterinarian monitoring during the study period of 4 weeks. Upon euthanasia 4 weeks after repair, no macroscopic signs of GI leaks were observed in any animals, despite partial (n = 3 animals; repaired by the GI patch without removable liner) or complete (n = 2 animals; repaired by the GI patch with removable liner) detachment of the GI patch. Histological evaluation of the repaired porcine colon by a blinded pathologist after 4 weeks indicated that the GI defects were fully healed with fibrotic tissue around them, without signs of granuloma or intramural abscess formation, for colons treated with GI patches with and without removable liner (Fig. 6, E and G, and fig. S21).

Other abdominal organs (liver, spleen, kidney, and untreated colon) in both treated groups were healthy, without evidence of inflammation or foreign body reaction (fig. S22). Defects repaired by the GI patch with removable liner exhibited more fibrosis around the defects as assessed histologically (Fig. 6E and fig. S21A) and had elevated collagen I, T cells (CD3), and macrophages per immunofluorescence staining and normalized immunofluorescence intensity analysis (Fig. 6F and fig. S23) compared with repair by the GI patch without a removable liner (Fig. 6, G and H, and fig. S23). These findings suggest that GI patches with or without removable liner can provide leak-free sutureless repair and healing of porcine colonic defects, but the GI patch without a removable liner appears to yield a more durable attachment and histologically more favorable outcome.

DISCUSSION

Whereas diverse factors contribute to postoperative GI leaks, the mechanical failure of surgically repaired GI defects and subsequent leakage of bowel contents is the most common etiology of GI leaks (*2*, *3*, *9*). Hence, various treatment strategies have been explored with the aim of improving mechanical sealing of GI defects through tissue adhesive sealants and/or structural reinforcement. Biologic (e.g., fibrin and gelatin) and synthetic (e.g., PEG, PU, and cyanoacrylate) forms of tissue adhesives and sealants have been developed and investigated

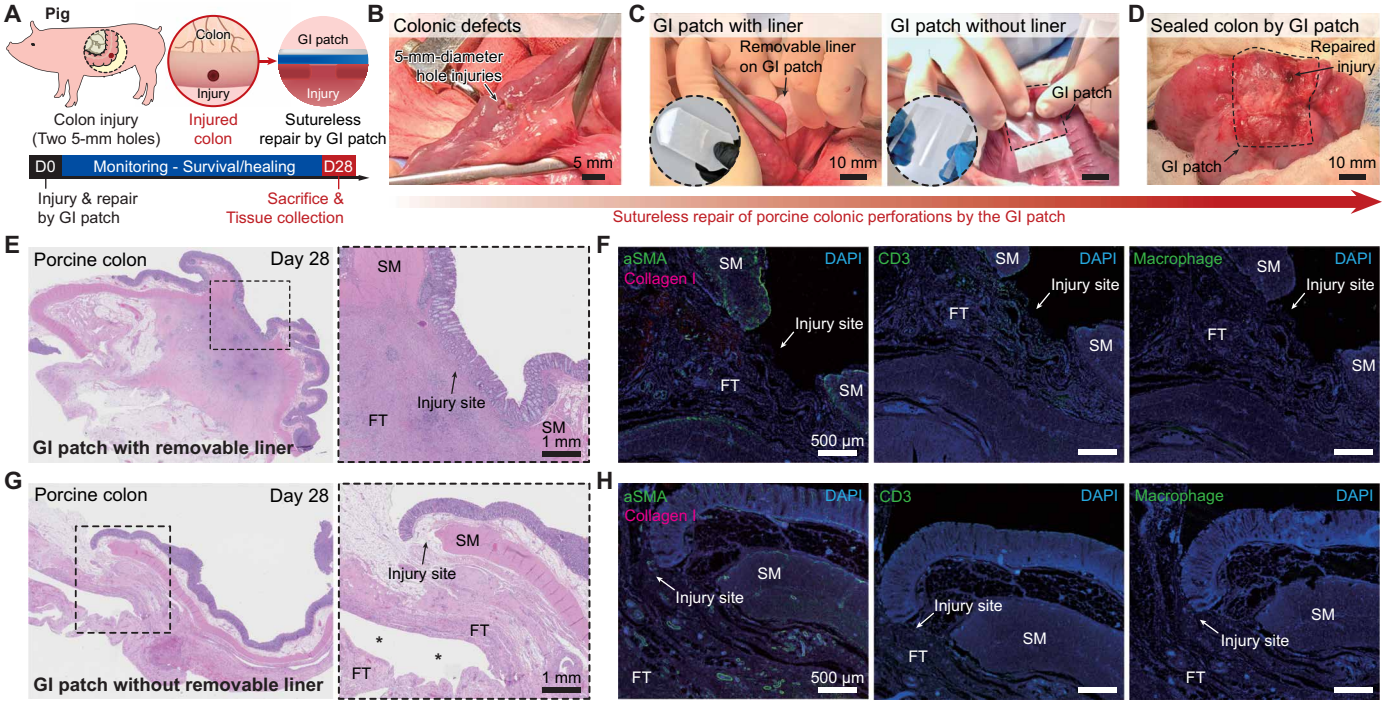

Fig. 6. Sutureless repair of GI defects in porcine model. (**A**) Schematic illustrations for in vivo sutureless repair of porcine colon defects by the GI patch. (**B** to **D**) Images for generation of two 5-mm-diameter defects in a porcine colon by a biopsy punch (B), sutureless repair of defects by the GI patch with (left) and without (right) removable liner (C), and sealed porcine colon defects by the GI patch (D). (**E** and **F**) Representative histological images stained with H&E (E) and immunofluorescence images (F) for porcine colon defects repaired by the GI patch with removable liner after 28 days. (**G** and **H**) Representative histological images stained with H&E (G) and immunofluorescence images (H) for porcine colon defects repaired by the GI patch without removable liner after 28 days. In histological images, * represents the GI patch; SM, smooth muscle; FT, fibrotic tissue. In immunofluorescence images, blue fluorescence corresponds to cell nuclei stained with DAPI; green fluorescence corresponds to the expression of fibroblast (aSMA, left), T cell (CD3, middle), and macrophage (right); red fluorescence corresponds to the expression of collagen I. Scale bars, 5 mm (B), 10 mm (C and D), 1 mm (E and G), and 500 μm (F and H).

for repair of GI defects in academic and commercial settings (*36*–*38*). However, existing tissue adhesives and sealants are fraught with limitations, including mechanical mismatch with GI tissues (e.g., cyanoacrylate), rapid degradation (e.g., fibrin and gelatin), and/or weak sealing strength (*11*, *38*–*41*). Mechanical reinforcement strategies have been explored using biologic patches (e.g., collagen) or synthetic buttresses (e.g., Seamguard and Gore). However, these mechanical reinforcement approaches have shown limited efficacy in preclinical studies (*42*–*44*). Overall, the limitations of existing technologies highlight the unmet clinical needs and the importance of developing new treatment solutions for repair of GI defects.

Mechanical failure of a structure and resultant leakage of fluidic contents within it is also a common problem in nonclinical applications (e.g., pipe leaks). Commercially available off-the-shelf products such as duct tapes are frequently used to form near-instant and robust fluid-tight sealing to prevent further leaks, providing both adhesive sealing and mechanical reinforcement to the structural defects (*45*). Despite not yet being developed for and incompatible with clinical and biomedical uses, the marked convenience and effectiveness of these off-the-shelf products such as duct tapes can provide valuable inspiration for the development of previously unknown solutions for the surgical repair of GI defects (*41*).

Here, we developed an off-the-shelf bioadhesive platform for atraumatic, facile, and robust repair of GI defects. Inspired by duct tapes, the GI patch integrates a nonadhesive top layer to provide mechanical reinforcement with a dry bioadhesive bottom layer to offer rapid and robust adhesion to the underlying GI tissue. This design and incorporation of the dry cross-linking mechanism render a preparation-free, ready-to-use GI patch. Here, comprehensive in vitro and in vivo biocompatibility evaluations showed that the GI patch exhibited biocompatibility comparable to that of U.S. Food and Drug Administration–approved commercially available tissue adhesive, such as Coseal, while being degradable long term (e.g., 12 weeks after implantation). Systematic characterizations of the GI patch using ex vivo porcine models identified tissue-matching mechanical properties and superior adhesive performance as compared with commercial tissue adhesives, sealants, and sutures.

However, our study also revealed some limitations and areas for future work. Although the GI patch provided facile sutureless sealing and anastomosis in rat models and colonic punch hole defects in a porcine model, the GI patch would require further validation and optimization for more geometrically and anatomically complex defects such as end-to-end anastomosis in large-animal models. It appears that the presence of the removable liner somewhat limited the haptic feedback during the patch application process due to higher stiffness and opacity and may have affected its adhesion performance. The adhesive performance, packaging, and application procedure of the GI patch may also benefit from further evaluation and optimization in close interaction with practicing surgeons to provide user-friendly haptic feedback and reproducible application and treatment efficacy. From a biomaterials perspective, the varying degree of inflammation and fibrosis as well as long-term stability of adhesion observed around the defects repaired by the GI patch in different species (i.e., rodent and porcine models) would require further in-depth investigation before clinical translation of the technology. Moreover, whereas the current study supports the in vivo degradability of the GI patch long term (e.g., 12 weeks after implantation), further fine-tuning of the degradation profile while considering the wound healing dynamic of GI defects may offer improved treatment efficacy (*35*). Despite its early developmental stage, the GI patch offers a promising off-the-shelf platform for atraumatic sutureless repair of GI defects that addresses limitations of previous approaches. We envision that the GI patch could also provide clinical opportunity for repair of other organs and injuries in the human body.

MATERIALS AND METHODS

Study design

The aim of this study was to develop an off-the-shelf bioadhesive in the form of a ready-to-use, thin, flexible, and transparent patch capable of providing rapid, fluid-tight, robust sealing of GI defects with straightforward application. We hypothesized that a tissue-like bioadhesive material with the aforementioned features could provide atraumatic and effective sealing and repair of GI defects and would address limitations and challenges of surgical repair using sutures. Systematic mechanical characterizations were performed using ex vivo porcine colon and stomach to evaluate adhesion (interface toughness, shear strength, tensile strength, and burst strength) to GI tissues in comparison with various commercially available tissue adhesives. In vitro LIVE/DEAD assay of human intestinal epithelial cell line (Caco-2) coculture for 24 hours was performed to evaluate cytotoxicity of the GI patch. In vivo biocompatibility of the GI patch was assessed on the basis of rat colon and stomach implantation models for 4 weeks followed by histopathological evaluation by a blinded pathologist, immunofluorescence analysis, qPCR analysis, and ELISA assay. In vivo degradability of the GI patch was investigated on the basis of a rat subcutaneous implantation model up to 12 weeks, assessing weight change of the implanted samples, histological evaluation, and blood analysis. In vivo efficacy of sutureless repair of GI defects by the GI patch was validated by rat colon, stomach, and small intestine defect-repair models and porcine colon defect-repair model for 4 weeks in comparison with a standard care control group based on sutures. The presence of leakage, sealing and healing of GI defects, and overall health of animals were assessed on the basis of animal monitoring, histopathological evaluation by a blinded pathologist, immunofluorescence analysis, qPCR analysis, and blood analysis. The appropriate sample size for each study was used on the basis of the literatures on similar evaluations. All tests were performed with randomly allocated experimental groups, and no data were excluded from the analyses.

Materials

All chemicals were obtained from Sigma-Aldrich unless otherwise mentioned and used without further purification. For preparation of the bioadhesive layer of the GI patch, acrylic acid (AAc), PVA (Mw = 146,000 to 186,000, 99+ % hydrolyzed), PEGDMA (Mn = 550), AAc-NHS ester, and α-ketoglutaric acid were used. For preparation of the nonadhesive layer of the GI patch, hydrophilic PU (HydroMed D3, AdvanSource Biomaterials) was used. As a removable liner for the GI patch, weighing paper (VWR) was used after autoclaving for sterilization. All porcine tissues and organs for ex vivo experiments were purchased from a research-grade porcine tissue vendor (Sierra Medical Inc.).

Preparation of the GI patch

To prepare the bioadhesive layer, 35 w/w % AAc, 7 w/w % PVA, 0.2 w/w % α-ketoglutaric acid, and 0.05 w/w % PEGDMA were added into

nitrogen-purged deionized water. Then, 30 mg of AAc-NHS ester was dissolved per 1 ml of the above stock solution to prepare a precursor solution (equivalent to 1% of dry bioadhesive weight). The precursor solution was then poured on a glass mold with spacers (150-μm thickness for rat study; 350-μm thickness for porcine study) and cured in a UV chamber (354 nm, 12 W power) for 30 min. To introduce the nonadhesive layer, 10 w/w % hydrophilic PU in ethanol solution (ethanol:water = 95:5 v/v) was spin coated on the as-prepared bioadhesive layer (200 rpm for rat study; 100 rpm for porcine study).

Prestretch (fig. S1A) equal to the equilibrium swelling ratio of the as-prepared bioadhesive was applied before drying the hydrophilic PU resin and bioadhesive layer following a previously reported method (*29*). The applied prestretch in the dry GI patch releases upon hydration of the bioadhesive layer and maintains the original size of the GI patch in the fully swollen state by canceling swelling of the bioadhesive layer (*29*) (fig. S3). Briefly, the as-prepared bioadhesive layer with the spin-coated PU solution was prestretched $\left(\lambda_{patch}^{pre} = \lambda_{bioadhesive}^{swelling} = 2.3\right)$ in both length and width directions. The prestretched sample was then dried under air flow for 1 hour followed by further drying in a vacuum desiccator chamber for 12 hours to prepare the dry GI patch. A removable liner was introduced for easier handling for rat studies and part of the porcine study. The dry GI patch was sealed in a sterile air-tight bag with desiccant and stored at room temperature before use.

Fourier transform infrared spectroscopy characterization

Chemical composition of the dry bioadhesive layer of the GI patch was characterized by a transmission Fourier transform infrared spectroscope (FTIR 6700, Thermo Fisher Scientific) using a Germanium attenuated total reflectance crystal (55°). Peaks for NHS ester groups (1158 and 1209 cm^{-1}) and carboxylic acid groups (1696 cm^{-1}) were identified in the absorbance versus wavenumber spectra based on the literature (*24*).

Mechanical characterization

Interfacial toughness was measured on the basis of the standard 180° peel test (ASTM F2256; fig. S8A). Shear strength was measured on the basis of the standard lap-shear test (ASTM F2255; fig. S8B). Tensile strength was measured on the basis of the standard tensile test (ASTM F2258; fig. S8C). The GI patch was applied to ex vivo porcine colon or stomach at 1-kPa pressure (applied either by mechanical testing machine or by equivalent weight) for 5 s. Commercially available tissue adhesives (Histoacryl, Coseal, and Tisseel) were applied between ex vivo porcine colon or stomach tissues following the testing standards. The application of commercially available tissue adhesives followed the provided user guide or manual for each product (measured after 1 min of application for Histoacryl, 3 min for Coseal, and 3 min for Tisseel). Before applying the GI patch or commercially available tissue adhesives, porcine tissues were covered with saline to ensure wetness of the tissues. For GI patch, mechanical tests were performed 5 min or 6 hours after initial application. All tests were performed using a mechanical testing machine (2.5 kN load-cell, Zwick/Roell Z2.5) at a constant crosshead speed of 50 mm min^{-1}. Poly(methyl methacrylate) films were applied using cyanoacrylate glue (Krazy Glue) to act as a stiff backing for the GI patch and porcine tissues. Aluminum fixtures were applied using cyanoacrylate glues to provide grips for tensile tests.

Ex vivo experiments

All ex vivo experiments were reviewed and approved by the Committee on Animal Care at the Massachusetts Institute of Technology (MIT). To demonstrate rapid and robust sutureless sealing of GI defects by the GI patch, two 5-mm-diameter defects were made by a biopsy punch to ex vivo porcine colon and stomach. Before applying the GI patch, porcine tissues were covered with saline to ensure wetness of the tissues. Then, the GI patch was applied on the defects by gentle pressing for 5 s. After repair by the GI patch, saline (blue colored by using a food dye) was injected to the porcine colon or stomach to evaluate fluid-tight sealing of the defects. To measure burst pressure, phosphate-buffered saline (PBS) was injected to the sealed porcine colon at the rate of 2 ml min^{-1} while the applied pressure was monitored by a pressure gauge (Omega) (modified ASTM F2392-04; fig. S8D).

In vitro biocompatibility

To evaluate in vitro biocompatibility and cytotoxicity of the GI patch, LIVE/DEAD assay was used to assess human intestinal epithelial cell line (Caco-2, American Type Culture Collection). To prepare conditioned media, 500 mg of Coseal, Histoacryl, and the swollen GI patch were incubated in 10 ml of Dulbecco's modified Eagle's medium (DMEM) supplemented with 10 v/v % fetal bovine serum and penicillin-streptomycin (100 U ml^{-1}) at 37°C for 24 hours. The supplemented DMEM without incubating tissue adhesive was used as a control. Caco-2 cells were plated in confocal dishes (20-mm diameter) at a density of 0.5×10^5 cells ($n = 4$ per each group). The cells were then treated with the control and conditioned media and incubated at 37°C for 24 hours in 5% CO_2 atmosphere. The cell viability was determined by a LIVE/DEAD viability/cytotoxicity kit for mammalian cells (Thermo Fisher Scientific) by adding 4 μM calcein and ethidium homodimer-1 into the culture media. A confocal microscope (SP 8, Leica) was used to image live cells with excitation/emission at 495 nm/515 nm and dead cells at 495 nm/635 nm, respectively. The cell viability was calculated by counting live (green fluorescence) and dead (red fluorescence) cells by using ImageJ (version 2.1.0).

In vivo biocompatibility and degradability

All animal studies on rat were approved by the MIT Committee on Animal Care, and all surgical procedures and postoperative care were supervised by MIT Division of Comparative Medicine veterinary staff. Female Sprague-Dawley rats (225 to 250 g, 12 weeks, Charles River Laboratories) were used for all in vivo studies. Before implantation, the GI patch was prepared using aseptic techniques and was further sterilized for 3 hours under UV light. Commercially available tissue adhesives were used as provided in sterile packages following the provided user guide or manual for each product.

For in vivo biocompatibility evaluation of the GI patch, the animals were anesthetized using isoflurane (2 to 3% isoflurane in oxygen) in an anesthetizing chamber before the surgery, and anesthesia was maintained using a nose cone throughout the surgery. Abdominal hair was removed, and the animals were placed on a heating pad during the surgery. Colon or stomach was exposed via a laparotomy. The GI patch (10 mm in width and 20 mm in length) was applied on the colon or stomach surface by gently pressing by a surgical spatula ($n = 4$). For commercially available tissue adhesives, 0.5 ml of Coseal ($n = 4$) and Histoacryl ($n = 4$) were injected on the colon or stomach surface. The abdominal wall muscle and skin incision was closed

using interrupted sutures, and 3 to 4 ml of warm saline was injected subcutaneously. Four weeks after the implantation, the animals were euthanized by CO_2 inhalation. Colon or stomach tissues of interest were excised and fixed in 10% formalin for 24 hours for histological and immunofluorescence analyses.

For in vivo degradability evaluation of the GI patch, the animals were anesthetized using isoflurane (2 to 3% isoflurane in oxygen) in an anesthetizing chamber before the surgery, and anesthesia was maintained using a nose cone throughout the surgery. The back hair was removed, and the animals were placed over a heating pad for the duration of the surgery. The dorsal subcutaneous space was accessed by a 1- to 2-cm skin incision per implant in the center of the animal's back. To create space for implant placement, blunt dissection was performed from the incision toward the animal shoulder blades. Both the GI patch (10 mm in diameter) and hydrophilic PU (10 mm in diameter) were placed in the two separate subcutaneous pockets in each rat ($n = 4$ for each time point). At 1, 4, 6, 8, 10, and 12 weeks after implantation time points, 3 to 5 ml of blood was collected via the cardiac puncture technique per animal for blood analysis, and the animals were euthanized by CO_2 inhalation. The implanted GI patch and hydrophilic PU were weighed, and subcutaneous regions of interest were excised and fixed in 10% formalin for 24 hours for histological analyses.

In vivo GI organ defect repair in rat model

For in vivo GI organ defect repair in the rat model, the animals were fasted for 24 hours before the surgery to minimize bowel contents in the colon and stomach. The animals were anesthetized using isoflurane (2 to 3% isoflurane in oxygen) in an anesthetizing chamber before the surgery, and anesthesia was maintained using a nose cone throughout the surgery. Abdominal hair was removed, and the animals were placed on a heating pad during the surgery. Colon or stomach was exposed via a median laparotomy. The exposed colon, stomach, or small intestine was packed with moistened sterile gauzes before creating a defect to prevent contamination of the abdominal cavity. A 10-mm incisional defect was made to the colon or stomach by using a scalpel and repaired by the GI patch (10 mm in width and 20 mm in length) or sutures (8-0 Prolene, Ethicon) ($n = 4$ for each group). For small intestine, 80 to 90% diameter of the small intestine was cut by using surgical scissors and repaired by the circumferentially applied GI patch (10 mm in width and 30 mm in length) or sutures (8-0 Prolene, Ethicon) ($n = 4$). After repair of the defect, warm saline was injected to the colon or stomach by a 32-gauge needle syringe to confirm the fluid-tight sealing. The abdominal wall muscle and skin incision were closed with sutures (4-0 Vicryl, Ethicon). One or 4 weeks after the repair, 3 to 5 ml of blood was collected via the cardiac puncture technique per animal for blood analysis, and then the animals were euthanized by CO_2 inhalation. Colon, stomach, or small intestine tissues of interest were inspected for postsurgical adhesion to the surrounding organs and excised and fixed in 10% formalin for 24 hours for histological and immunofluorescence analyses. All animals in the study were survived and kept in normal health conditions based on daily monitoring by the MIT Department of Comparative Medicine (DCM) veterinarian staff.

In vivo colon defect repair in porcine model

All animal studies on pig were approved by the Mayo Clinic institutional animal care and use committee (IACUC) at Rochester. The female domestic pigs (40 to 55 kg, 20 weeks, Manthei Hog Farm) were fasted for 24 hours before the surgery to minimize bowel contents in the descending colon. The animals were placed in dorsal recumbency, and the abdominal region was clipped and prepared aseptically. A blade was used to incise on the ventral midline and extended using electrocautery when indicated. The linea alba was incised and peritoneum bluntly entered, with the incision extended to match the skin incision. The spiral colon was exteriorized, and moist lap sponges were used for isolation. Colonic ingesta were milked away from the intended surgical site, and side-biting intestinal clamps were applied to isolate a portion of the colonic wall. A 5-mm-diameter biopsy punch was used to create two lesions in the colon wall to mimic anastomotic leak with free access to ingesta to the abdominal cavity. Then, a GI patch was applied and adhered over the biopsied region to create a seal ($n = 2$ animals for the GI patch with removable liner; $n = 3$ animals for the GI patch without removable liner). The colon was thoroughly lavaged and returned to the abdomen, and then the entire abdominal cavity was lavaged and suctioned before the celiotomy incision was closed. Four weeks after the repair, the animals were humanely euthanized, and the wound region sealed by the GI patch was excised and fixed in 10% formalin for 24 hours for histological and immunofluorescence analyses. All animals in the study were survived and kept in normal health conditions based on daily monitoring by the Mayo Clinic Rochester veterinarian staff.

Histology and immunofluorescence

Fixed tissue samples were placed into 70% ethanol and submitted for histological processing and hematoxylin and eosin (H&E) or Masson's trichrome staining at the Hope Babette Tang (1983) Histology Facility in the Koch Institute for Integrative Cancer Research at the MIT. Histological assessment was performed by a blinded pathologist, and representative images of each group were shown in the corresponding figures.

For immunofluorescence, paraffin sections of the fixed tissues were cut at 5-μm thickness and baked in 50°C overnight. The tissue sections were then deparaffinized, rehydrated with deionized water, and underwent antigen retrieval using the steam method. Then, the slides were washed in three changes of PBS–Tween 20 for 5 min per cycle. After washing, the slides were incubated in primary antibodies [mouse anti-aSMA for fibroblast (1:200; ab7817, Abcam); mouse anti-CD68 for macrophages (1:200; ab201340, Abcam); rabbit anti-CD3 for T cells (1:100; ab5690, Abcam); rabbit anti–collagen I for collagen (1:200; ab21286, Abcam); rabbit anti-iNOS (1:2000; ab283655, Abcam); rabbit anti-CD206 (1:1000; ab64693, Abcam); mouse anti-vimentin (1:500; ab8978, Abcam); rabbit anti–collagen III (1:1000; ab283694, Abcam); mouse anti-CD3 (1:40; LifeSpan, LS-C350938); and mouse anti-macrophages (1:40; MCA2317GA, Bio-Rad)] diluted with IHC-Tek antibody diluent for 1 hour at room temperature. The slides were then washed three times with PBS–Tween 20 and incubated with Alexa Fluor 488 donkey anti-mouse (1:200; Jackson Immuno Research) or Alexa Fluor 594 donkey anti-rabbit secondary antibody (1:200; Jackson Immuno Research) at room temperature in a dark environment for 30 min. The slides were washed in PBS–Tween 20 three times for 5 min per cycle. Then, the slides were incubated with fluorescent mounting medium with 4′,6-diamidino-2-phenylindole (DAPI), and the edge was sealed with a nail polish. A laser confocal microscope (SP8, Leica) was used for image acquisition. ImageJ (version 2.1.0) was used to quantify the fluorescence intensity of

expressed antibodies. All the images were transformed to the 8-bit binary images, and the fluorescence intensity was calculated with normalized analysis. All analyses were blinded with respect to the experimental conditions.

ELISA assay

Tissues were harvested and homogenized on ice in lysis buffer containing protease inhibitor cocktail. After centrifugation at 10,000*g* for 10 min at 4°C, the supernatants were collected for the detection of TNF-α and IL-6 cytokines activity using ELISA kits according to the manufacturer's instructions (BioLegend, USA).

qPCR analysis

RNA was isolated from samples snap frozen in liquid nitrogen immediately after excision using the TRIzol protocol (Invitrogen, USA). All samples were homogenized and normalized by loading 2 μg of total RNA in all cases for reverse transcription using a SuperScript First Strand cDNA Synthesis Kit (Invitrogen, USA). Complementary DNA (1:20 dilution) was amplified by qPCR with the following primers: *Mrc1* (5′-AACTTCATCTGCCAGCGACA-3′; reverse: 5′-CGTGCCTCTTTCCAGGTCTT-3′), *Tgfb1* (5′-AGTGGCTGAACCAAGGAGAC-3′; reverse: 5′-CCTCGACGTTTGGGACTGAT-3′), *Nos2* (5′-TGGTGAGGGGACTGGACTTT-3′; reverse: 5′-CCAACTCTGCTGTTCTCCGT-3′), *Cd86* (5′-AGACATGTGTAACCTGCACCAT-3′; reverse: 5′-TACGAGCTCACTCGGGCTTA-3′), Arg1 (5′-TGTGCCCTCTGTCTTTTAGGG-3′; reverse: 5′-GCTCATGCTCATCCAGGGTT-3′), *Col1a1* (5′-ATGCTGAATCGTCCCACCAG-3′; reverse: 5′-ATGTCCCGGCAGGATTTGAA-3′), *Col3a1* (5′-AGGGCAGGGAACAACTGATG-3′; reverse: 5′-GGTCCCACATTGCACAAAGC-3′), *Acta2* (5′-GGATCAGCGCCTTCAGTTCT-3′; reverse: 5′-AGGGCTAGAAGGGTAGCACA-3′), *IL2* (5′-CCAAGCAGGCCACAGAATTG; reverse: 5′-TCCAGCGTCTTCCAAGTGAA-3′), and glyceraldehyde-3-phosphate dehydrogenase (*GAPDH*) (5′-CACCATCTTCCAGGAGCGAG-3′; reverse: 5′-CCACGACATACTCAGCACCA-3′). Samples were incubated for 10 min at 95°C for 15 s and at 60°C for 1 min in the real-time cycler Agilent MX3000P. *GAPDH* was used as reference gene for normalization and analysis. Comparative C_T ($\Delta\Delta C_T$) method was used for relative quantification of gene expression.

Statistical analysis

GraphPad Prism (version 9.2.0) was used to assess the statistical significance of all comparison studies in this work. Data distribution was assumed to be normal for all parametric tests but not formally tested. In the statistical analysis for comparison between multiple groups, one-way analysis of variance (ANOVA) followed by Bonferroni's multiple comparison test was conducted with the significance threshold of $^*P < 0.05$, $^{**}P \leq 0.01$, and $^{***}P \leq 0.001$. In the statistical analysis between two groups, the two-sided Student's *t* test was used with the significance threshold of $^*P < 0.05$, $^{**}P \leq 0.01$, and $^{***}P \leq 0.001$.

SUPPLEMENTARY MATERIALS

www.science.org/doi/10.1126/scitranslmed.abh2857
Figs. S1 to S23
MDAR Reproducibility Checklist
Data files S1 to S5
Movies S1 to S5

View/request a protocol for this paper from *Bio-protocol*.

REFERENCES AND NOTES

1. F. Marra, T. Steffen, N. Kalak, R. Warschkow, I. Tarantino, J. Lange, M. Zünd, Anastomotic leakage as a risk factor for the long-term outcome after curative resection of colon cancer. *Eur. J. Surg. Oncol.* **35**, 1060–1064 (2009).
2. H. M. Halawani, W. Faraj, G. Khoury, F. Khalifeh, S. Deeba, Colorectal anastomotic leaks: A brief review of current literature. *World J. Colorectal Surg.* **4**, 4 (2015).
3. F. Daams, M. Luyer, J. F. Lange, Colorectal anastomotic leakage: Aspects of prevention, detection and treatment. *World J Gastroenterol: WJG* **19**, 2293–2297 (2013).
4. J. Hammond, S. Lim, Y. Wan, X. Gao, A. Patkar, The burden of gastrointestinal anastomotic leaks: An evaluation of clinical and economic outcomes. *J. Gastrointest. Surg.* **18**, 1176–1185 (2014).
5. A. Schiff, B. L. Brady, S. K. Ghosh, S. Roy, C. Ruetsch, E. Fegelman, Estimated rate of post-operative anastomotic leak following colorectal resection surgery: A systematic review. *J. Surg. Surgical Res.* **2**, 60–67 (2015).
6. D. E. Huisman, M. Reudink, S. J. van Rooijen, B. T. Bootsma, T. van de Brug, J. Stens, W. Bleeker, L. P. S. Stassen, A. Jongen, C. V. Feo, S. Targa, N. Komen, H. M. Kroon, T. Sammour, E. A. G. L. Lagae, A. K. Talsma, J. A. Wegdam, T. S. de Vries Reilingh, B. van Wely, M. J. van Hoogstraten, D. J. A. Sonneveld, S. C. Veltkamp, E. G. G. Verdaasdonk, R. M. H. Roumen, G. D. Slooter, F. Daams, LekCheck: A prospective study to identify perioperative modifiable risk factors for anastomotic leakage in colorectal surgery. *Ann. Surg.* **257**, e189–e197 (2022).
7. N. Annabi, K. Yue, A. Tamayol, A. Khademhosseini, Elastic sealants for surgical applications. *Eur. J. Pharm. Biopharm.* **95**, 27–39 (2015).
8. G. M. Taboada, K. Yang, M. J. N. Pereira, S. S. Liu, Y. Hu, J. M. Karp, N. Artzi, Y. Lee, Overcoming the translational barriers of tissue adhesives. *Nat. Rev. Mater.* **5**, 310–329 (2020).
9. J. C. Slieker, F. Daams, I. M. Mulder, J. Jeekel, J. F. Lange, Systematic review of the technique of colorectal anastomosis. *JAMA Surg.* **148**, 190–201 (2013).
10. D. A. Wang, S. Varghese, B. Sharma, I. Strehin, S. Fermanian, J. Gorham, D. H. Fairbrother, B. Cascio, J. H. Elisseeff, Multifunctional chondroitin sulphate for cartilage tissue–biomaterial integration. *Nat. Mater.* **6**, 385–392 (2007).
11. T. Vuocolo, R. Haddad, G. A. Edwards, R. E. Lyons, N. E. Liyou, J. A. Werkmeister, J. A. M. Ramshaw, C. M. Elvin, A highly elastic and adhesive gelatin tissue sealant for gastrointestinal surgery and colon anastomosis. *J. Gastrointest. Surg.* **16**, 744–752 (2012).
12. B. Sharma, S. Fermanian, M. Gibson, S. Unterman, D. A. Herzka, B. Cascio, J. Coburn, A. Y. Hui, N. Marcus, G. E. Gold, J. H. Elisseeff, Human cartilage repair with a photoreactive adhesive-hydrogel composite. *Sci. Transl. Med.* **5**, 167ra166 (2013).
13. N. Lang, M. J. Pereira, Y. Lee, I. Friehs, N. V. Vasilyev, E. N. Feins, K. Ablasser, E. D. O'Cearbhaill, C. Xu, A. Fabozzo, R. Padera, S. Wasserman, F. Freudenthal, L. S. Ferreira, R. Langer, J. M. Karp, P. J. del Nido, A blood-resistant surgical glue for minimally invasive repair of vessels and heart defects. *Sci. Transl. Med.* **6**, 218ra216 (2014).
14. N. Annabi, Y.-N. Zhang, A. Assmann, E. S. Sani, G. Cheng, A. D. Lassaletta, A. Vegh, B. Dehghani, G. U. Ruiz-Esparza, X. Wang, S. Gangadharan, A. S. Weiss, A. Khademhosseini, Engineering a highly elastic human protein–based sealant for surgical applications. *Sci. Transl. Med.* **9**, eaai7466 (2017).
15. E. S. Sani, A. Kheirkhah, D. Rana, Z. Sun, W. Foulsham, A. Sheikhi, A. Khademhosseini, R. Dana, N. Annabi, Sutureless repair of corneal injuries using naturally derived bioadhesive hydrogels. *Sci. Adv.* **5**, eaav1281 (2019).
16. X. Lin, Y. Liu, A. Bai, H. Cai, Y. Bai, W. Jiang, H. Yang, X. Wang, L. Yang, N. Sun, H. Gao, A viscoelastic adhesive epicardial patch for treating myocardial infarction. *Nat. Biomed. Eng.* **3**, 632–643 (2019).
17. L. M. Stapleton, A. N. Steele, H. Wang, H. L. Hernandez, A. C. Yu, M. J. Paulsen, A. A. A. Smith, G. A. Roth, A. D. Thakore, H. J. Lucian, K. P. Totherow, S. W. Baker, Y. Tada, J. M. Farry, A. Eskandari, C. E. Hironaka, K. J. Jaatinen, K. M. Williams, H. Bergamasco, C. Marschel, B. Chadwick, F. Grady, M. Ma, E. A. Appel, Y. J. Woo, Use of a supramolecular polymeric hydrogel as an effective post-operative pericardial adhesion barrier. *Nat. Biomed. Eng.* **3**, 611–620 (2019).
18. A. M. Behrens, N. G. Lee, B. J. Casey, P. Srinivasan, M. J. Sikorski, J. L. Daristotle, A. D. Sandler, P. Kofinas, Biodegradable-polymer-blend-based surgical sealant with body-temperature-mediated adhesion. *Adv. Mater.* **27**, 8056–8061 (2015).
19. N. G. Kern, A. M. Behrens, P. Srinivasan, C. T. Rossi, J. L. Daristotle, P. Kofinas, A. D. Sandler, Solution blow spun polymer: A novel preclinical surgical sealant for bowel anastomoses. *J. Pediatr. Surg.* **52**, 1308–1312 (2017).
20. J. L. Daristotle, S. T. Zaki, L. W. Lau, O. B. Ayyub, M. Djouini, P. Srinivasan, M. Erdi, A. D. Sandler, P. Kofinas, Pressure-sensitive tissue adhesion and biodegradation of viscoelastic polymer blends. *ACS Appl. Mater. Interfaces* **12**, 16050–16057 (2020).
21. X. Xu, X. Xia, K. Zhang, A. Rai, Z. Li, P. Zhao, K. Wei, L. Zou, B. Yang, W.-K. Wong, P. W.-Y. Chiu, L. Bian, Bioadhesive hydrogels demonstrating pH-independent

and ultrafast gelation promote gastric ulcer healing in pigs. *Sci. Transl. Med.* **12**, eaba8014 (2020).
22. H. Yuk, T. Zhang, S. Lin, G. A. Parada, X. Zhao, Tough bonding of hydrogels to diverse non-porous surfaces. *Nat. Mater.* **15**, 190–196 (2016).
23. H. Yuk, C. E. Varela, C. S. Nabzdyk, X. Mao, R. F. Padera, E. T. Roche, X. Zhao, Dry double-sided tape for adhesion of wet tissues and devices. *Nature* **575**, 169–174 (2019).
24. X. Chen, H. Yuk, J. Wu, C. S. Nabzdyk, X. Zhao, Instant tough bioadhesive with triggerable benign detachment. *Proc. Natl. Acad. Sci.* **117**, 15497–15503 (2020).
25. J. Li, A. D. Celiz, J. Yang, Q. Yang, I. Wamala, W. Whyte, B. R. Seo, N. V. Vasilyev, J. J. Vlassak, Z. Suo, D. J. Mooney, Tough adhesives for diverse wet surfaces. *Science* **357**, 378–381 (2017).
26. J. Yang, R. Bai, Z. Suo, Topological adhesion of wet materials. *Adv. Mater.* **30**, 1800671 (2018).
27. X. Mao, H. Yuk, X. Zhao, Hydration and swelling of dry polymers for wet adhesion. *J. Mech. Phys. Solids* **137**, 103863 (2020).
28. J. Deng, H. Yuk, J. Wu, C. E. Varela, X. Chen, E. T. Roche, C. F. Guo, X. Zhao, Electrical bioadhesive interface for bioelectronics. *Nat. Mater.* **20**, 229–236 (2021).
29. G. Theocharidis, H. Yuk, H. Roh, L. Wang, I. Mezghani, J. Wu, A. Kafanas, L. Chen, C. F. Guo, N. Jayaswal, X.-L. Katopodi, C. S. Nabzdyk, I. S. Vlachos, A. Veves, X. Zhao, Strain-programmable patch for diabetic wound healing. *bioRxiv* 10.1101/2021.1106.1107.447423 , (2021).
30. X. Li, X. J. Loh, K. Wang, C. He, J. Li, Poly (ester urethane) s consisting of poly [(R)-3-hydroxybutyrate] and poly (ethylene glycol) as candidate biomaterials: Characterization and mechanical property study. *Biomacromolecules* **6**, 2740–2747 (2005).
31. X. J. Loh, K. K. Tan, X. Li, J. Li, The in vitro hydrolysis of poly (ester urethane) s consisting of poly [(R)-3-hydroxybutyrate] and poly (ethylene glycol). *Biomaterials* **27**, 1841–1850 (2006).
32. B. R. Freedman, O. Uzun, N. M. M. Luna, A. Rock, C. Clifford, E. Stoler, G. Östlund-Sholars, C. Johnson, D. J. Mooney, Degradable and removable tough adhesive hydrogels. *Adv. Mater.* **33**, 2008553 (2021).
33. L. Van De Water, S. Varney, J. J. Tomasek, Mechanoregulation of the myofibroblast in wound contraction, scarring, and fibrosis: Opportunities for new therapeutic intervention. *Adv. Wound Care* **2**, 122–141 (2013).
34. E. Dondossola, B. M. Holzapfel, S. Alexander, S. Filippini, D. W. Hutmacher, P. Friedl, Examination of the foreign body response to biomaterials by nonlinear intravital microscopy. *Nat. Biomed. Eng.* **1**, 0007 (2017).
35. M. J. Koruda, R. H. Rolandelli, Experimental studies on the healing of colonic anastomoses. *J. Surg. Res.* **48**, 504–515 (1990).
36. K. A. Vakalopoulos, F. Daams, Z. Wu, L. Timmermans, J. J. Jeekel, G.-J. Kleinrensink, A. Ham, J. F. Lange, Tissue adhesives in gastrointestinal anastomosis: A systematic review. *J. Surg. Res.* **180**, 290–300 (2013).
37. M. A. Stam, C. L. J. Mulder, E. C. J. Consten, J. B. Tuynman, C. J. Buskens, W. A. Bemelman, Sylys® surgical sealant: A safe adjunct to standard bowel anastomosis closure. *Annals Surg. Innov. Res.* **8**, 6 (2014).
38. Y. Kopelman, Y. Nir, Y. Siman-Tov, B. Person, O. Zmora, A gelatin-based prophylactic sealant for bowel wall closure, initial evaluation in mid-rectal anastomosis in a large animal model. *J. Gastroint. Dig. Syst.* **5**, 258 (2015).
39. S. Truong, G. Böhm, U. Klinge, M. Stumpf, V. Schumpelick, Results after endoscopic treatment of postoperative upper gastrointestinal fistulas and leaks using combined Vicryl plug and fibrin glue. *Surg. Endosc. Other Interv. Tech.* **18**, 1105–1108 (2004).
40. K. A. Vakalopoulos, Z. Wu, L. Kroese, G.-J. Kleinrensink, J. Jeekel, R. Vendamme, D. Dodou, J. F. Lange, Mechanical strength and rheological properties of tissue adhesives with regard to colorectal anastomosis: An ex vivo study. *Ann. Surg.* **261**, 323–331 (2015).
41. A. H. C. Anthis, X. Hu, M. T. Matter, A. L. Neuer, K. Wei, A. A. Schlegel, F. H. L. Starsich, I. K. Herrmann, Chemically stable, strongly adhesive sealant patch for intestinal anastomotic leakage prevention. *Adv. Funct. Mater.* **31**, 2007099 (2021).
42. T. Nordentoft, J. Rømer, M. Sørensen, Sealing of gastrointestinal anastomoses with a fibrin glue-coated collagen patch: A safety study. *J. Invest. Surg.* **20**, 363–369 (2007).
43. W. W. Hope, M. Zerey, T. M. Schmelzer, W. L. Newcomb, B. L. Paton, J. J. Heath, R. D. Peindl, H. J. Norton, A. E. Lincourt, B. T. Heniford, K. S. Gersin, A comparison of gastrojejunal anastomoses with or without buttressing in a porcine model. *Surg. Endosc.* **23**, 800–807 (2009).
44. L. Tallón-Aguilar, F. A. Lopez-Bernal, J. Muntane-Relat, J. A. García-Martínez, E. Castillo-Sanchez, J. Padillo-Ruiz, The use of TachoSil as sealant in an experimental model of colonic perforation. *Surg. Innov.* **22**, 54–60 (2015).
45. C. Creton, Pressure-sensitive adhesives: An introductory course. *MRS Bull.* **28**, 434–439 (2003).

Acknowledgments: We thank the Koch Institute Swanson Biotechnology Center for technical support, specifically K. Cormier, and the Histology Core for the histological processing. We thank J. Arnold and B. Berger at MIT Deshpande Center for the insightful discussion on the bioadhesive applications for GI defect repair, R. Bronson at Harvard Medical School for the histological analyses, and X. Chen at MIT for help in the FTIR analysis. **Funding:** The work was supported by the MIT Deshpande Center and the Centers for Mechanical Engineering Research and Education at MIT and SUSTech. H.Y. acknowledges financial support from a Samsung scholarship. **Author contributions:** H.Y., J.W., C.S.N., and X.Z. conceived the idea for the GI patch. H.Y., J.W., C.S.N., L.G.G., T.L.S., and X.Z. designed the research. H.Y. and J.W. developed the materials and method for the GI patch. H.Y., J.W., C.F.G., and C.S.N. designed the in vitro and ex vivo experiments. H.Y. and J.W. conducted the in vitro and ex vivo experiments and analysis. J.W., H.Y., C.S.N., and X.Z. designed the in vivo experiments. J.W. and H.Y. conducted the in vivo rat studies and analysis. C.S.N., T.L.S., and L.G.G. designed and conducted the in vivo pig studies and analysis. X.Z. and C.S.N. supervised the study. All authors wrote the manuscript. **Competing interests:** H.Y. and X.Z. are inventors on the patent describing the bioadhesive patch (US 2020/0353120). H.Y., C.S.N., and X.Z. have a financial interest in SanaHeal Inc., a biotechnology company focused on the development of medical devices for surgical sealing and repair. The authors declare that they have no other competing interests. **Data and materials availability:** All data associated with this study are present in the paper or in the Supplementary Materials.

Submitted 26 February 2021
Resubmitted 3 November 2021
Accepted 13 January 2022
Published 2 February 2022
10.1126/scitranslmed.abh2857

Science Translational Medicine

An off-the-shelf bioadhesive patch for sutureless repair of gastrointestinal defects

Jingjing WuHyunwoo YukTiffany L. SarrafianChuan Fei GuoLeigh G. GriffithsChristoph S. NabzdykXuanhe Zhao

Sci. Transl. Med., 14 (630), eabh2857.

Sealing the deal

Tissue sealants and adhesives are potentially useful alternatives to sutures for tissue repair, but application to wet tissue can be complex or take too long to set during surgery. Wu *et al.* developed a flexible, transparent adhesive polymer hydrogel patch that seals gastric tissue defects. The patch could be applied to wet tissue and showed strong adhesion shortly after application and when fully swollen (6 hours after application). Patches sealed defects in rat colon, stomach, and small intestine, promoting tissue healing and maintaining adhesion over 4 weeks. The technology could be scaled to seal defects in pig colon. Results support further investigation of this easy-to-apply patch as an alternative to commercially available tissue adhesives.

Science Translational Medicine (ISSN) is published by the American Association for the Advancement of Science. 1200 New York Avenue NW, Washington, DC 20005. The title *Science Translational Medicine* is a registered trademark of AAAS.

Science Translational Medicine
AAAS

Supplementary Materials for

An off-the-shelf bioadhesive patch for sutureless repair of gastrointestinal defects

Jingjing Wu *et al.*

Corresponding author: Hyunwoo Yuk, hyunwoo@mit.edu; Leigh G. Griffiths, griffiths.leigh@mayo.edu,

Christoph S. Nabzdyk, nabzdyk.christoph@mayo.edu; Xuanhe Zhao, zhaox@mit.edu

Sci. Transl. Med. **14**, eabh2857 (2022)
DOI: 10.1126/scitranslmed.abh2857

The PDF file includes:

Other Supplementary Material for this manuscript includes the following:

SUPPLEMENTARY MATERIALS

Supplementary Figures

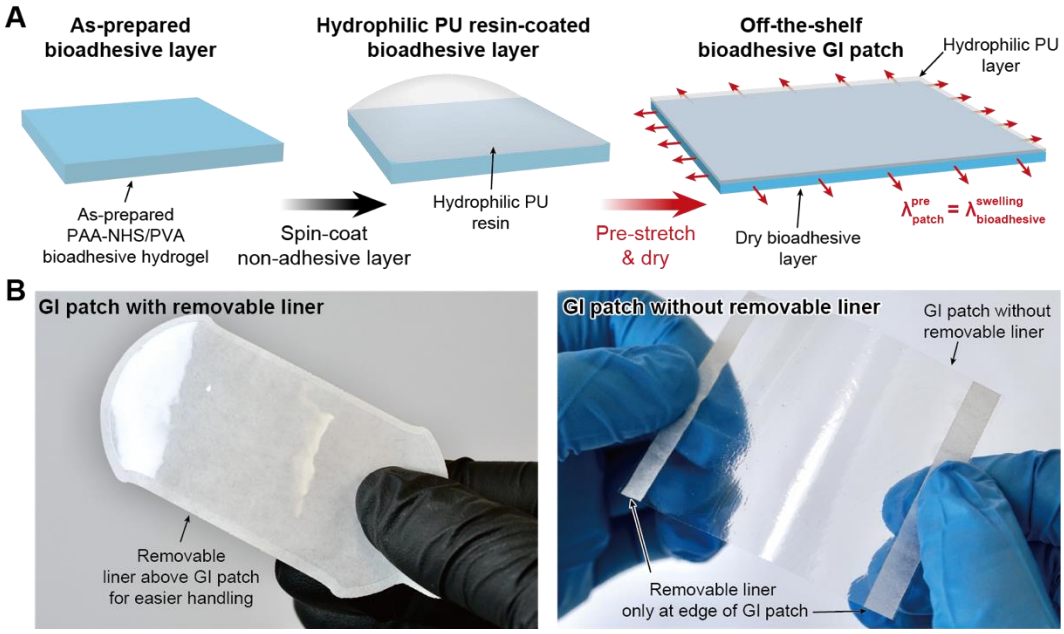

Fig. S1. Off-the-shelf bioadhesive GI patch. (**A**) Schematic detailing the fabrication process of the GI patch. PU, polyurethane; $\lambda^{\text{pre}}_{\text{patch}}$, applied pre-stretch; $\lambda^{\text{swelling}}_{\text{bioadhesive}}$, equilibrium swelling ratio of the bioadhesive. (**B**) Photographs of dry GI patch with (left) and without (right) removable liner.

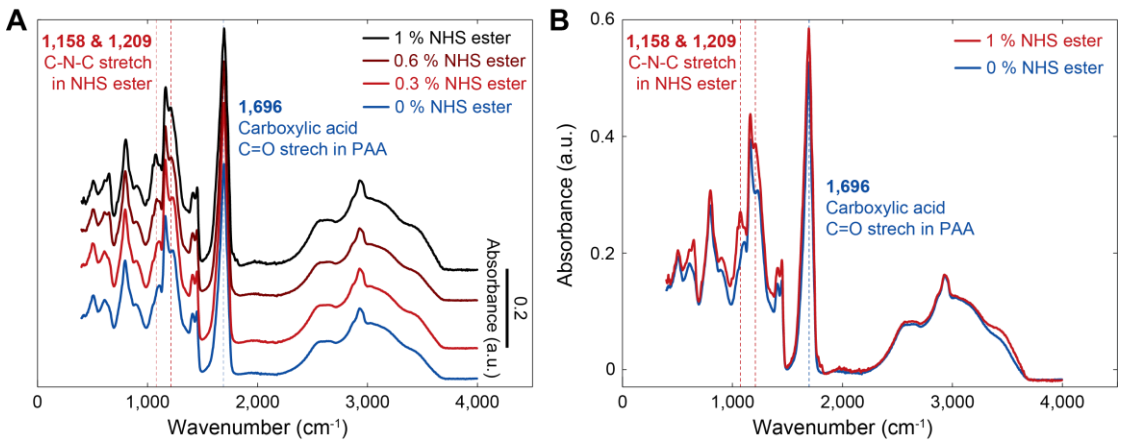

Fig. S2. FTIR analysis of the dry bioadhesive layer. (**A**) FTIR absorbance vs. wavenumber spectra for the dry bioadhesive layer of the GI patch with varying NHS ester concentration at 0, 0.3, 0.6, and 1 % of the dry bioadhesive weight. (**B**) FTIR absorbance vs. wavenumber spectra for the dry bioadhesive layer of the GI patch without NHS ester (0 % of the dry bioadhesive weight) and with NHS ester (1 % of the dry bioadhesive weight). In FTIR spectra, peaks at 1,158 and 1,209 cm^{-1} correspond to C-N-C stretch in NHS ester groups; peaks at 1,696 cm^{-1} correspond to C=O stretch of carboxylic acid groups in PAA.

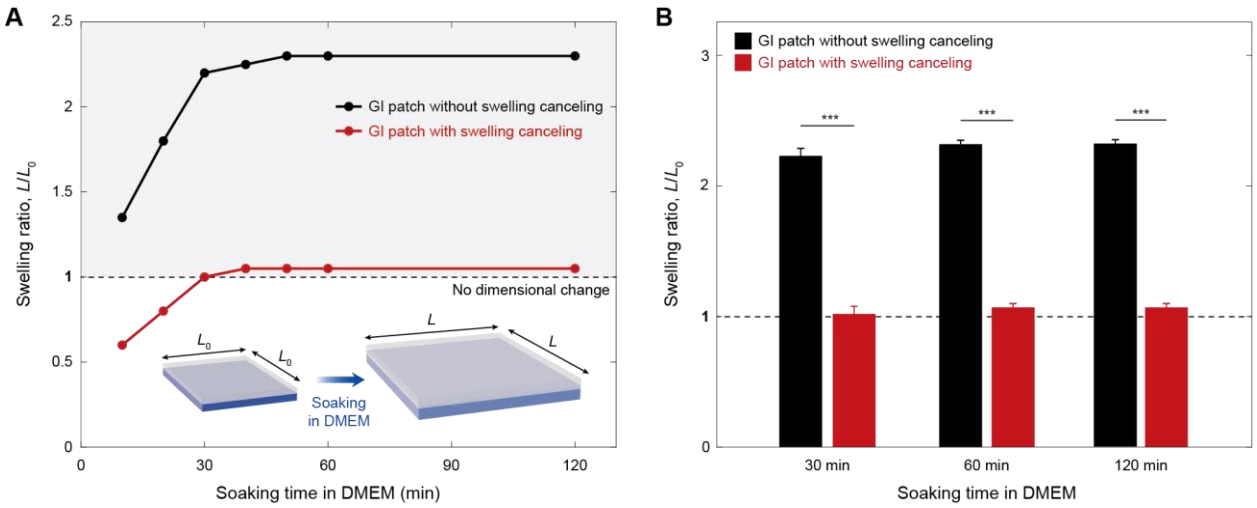

Fig. S3. Swelling property of the GI patch. (**A**) Swelling ratio of the GI patch prepared without and with pre-stretch to cancel swelling over time in DMEM at 37 ℃. DMEM, Dulbecco's Modified Eagle Medium. (**B**) Swelling ratio of the GI patch prepared without and with pre-stretch to cancel swelling in DMEM at 37 ℃ after 30, 60, and 120 min. Values in B represent the means ± SD (n = 3). P values are determined by two-sided t test; *** $P \leq 0.001$.

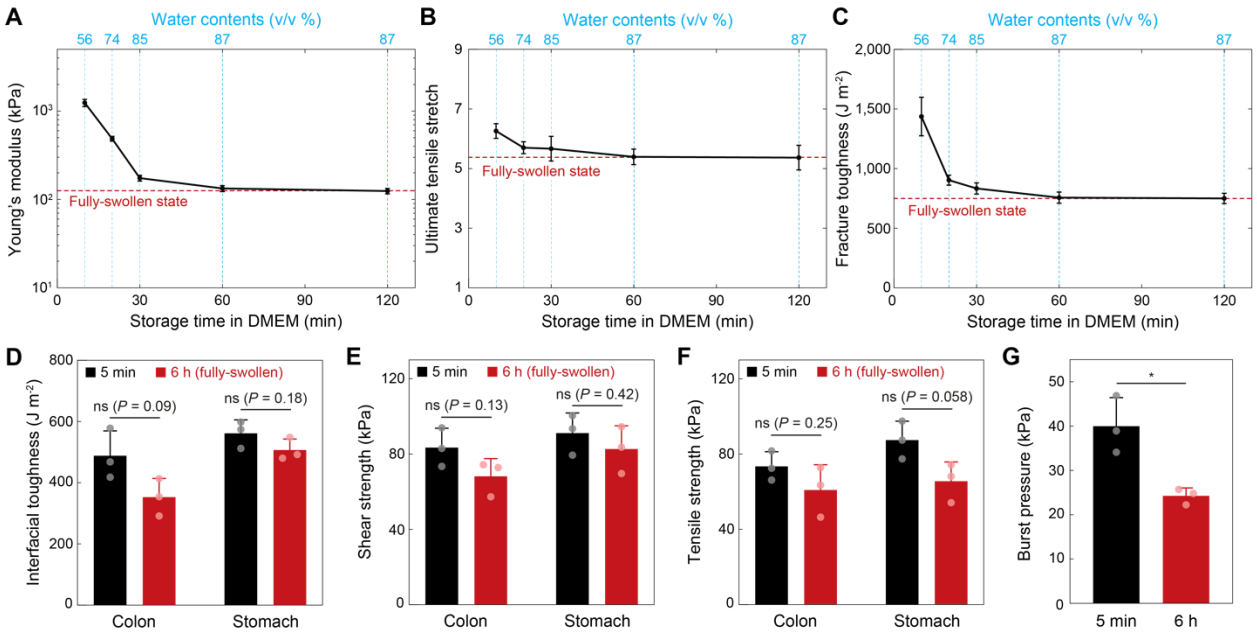

Fig. S4. Mechanical properties of the GI patch during swelling. (**A** to **C**) Young's modulus (A), ultimate tensile stretch (B), and fracture toughness (C) of the GI patch with varying water contents. Red dotted lines represent the values at the fully swollen state. (**D** to **G**) Interfacial toughness (D), shear strength (E), tensile strength (F), and burst pressure (G) of the GI patch on ex vivo porcine GI tissues measured 5 min and 6 h after the initial application. Values represent the means ± SD (n = 3). P values are determined by two-sided t test; ns, not significant; * $P < 0.05$.

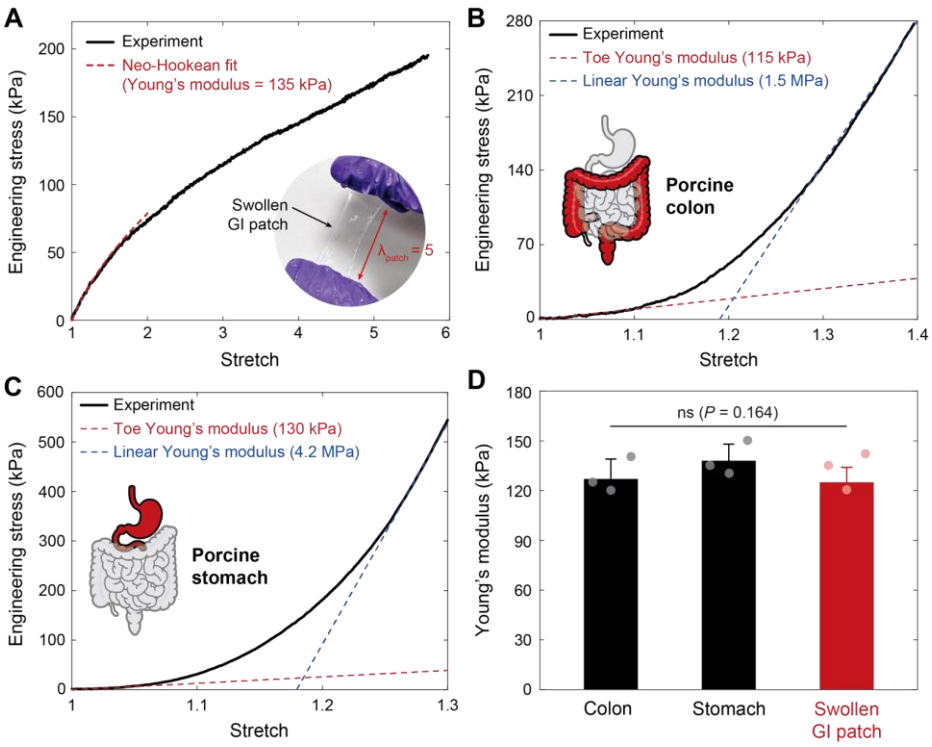

Fig. S5. Mechanical properties of the swollen GI patch and porcine GI organs. (**A**) Engineering stress vs stretch curve for the swollen GI patch under tensile deformation. Inset image shows the swollen GI patch stretched 5 times of the original length. (**B** and **C**) Engineering stress vs stretch curves for ex vivo porcine colon (B) and stomach (C) under tensile loading. (**D**) Young's moduli of porcine colon, porcine stomach, and the swollen GI patch. Values in D represent the means ± SD (n = 3). P values are determined by one-way ANOVA followed by the Bonferroni's multiple comparison test; ns, not significant.

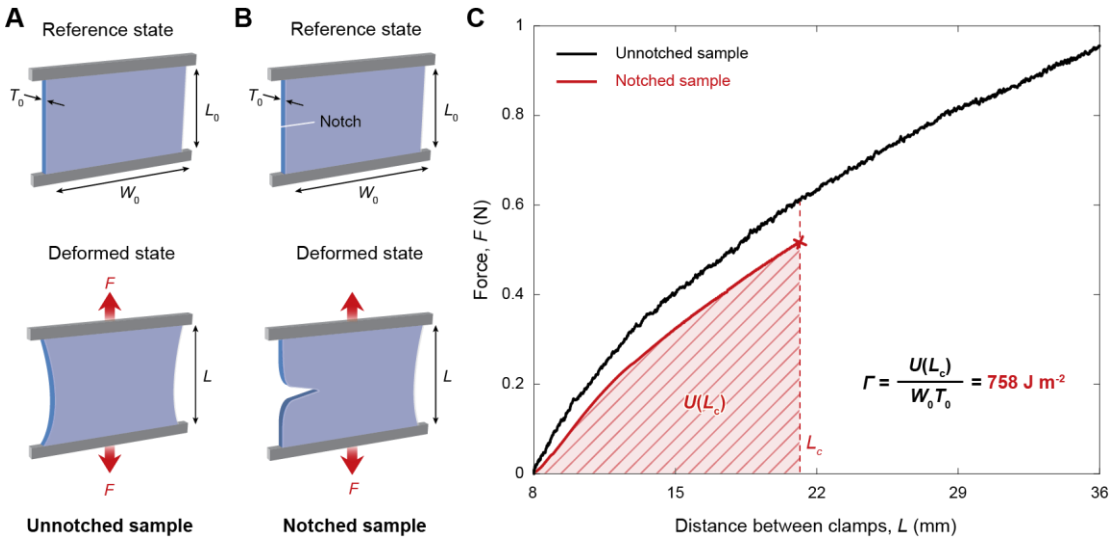

Fig. S6. Fracture toughness of the GI patch. (**A** and **B**) Schematic illustrations of pure-shear test for an unnotched sample (A) and a notched sample (B). (**C**) Force vs. distance between clamps for the unnotched and notched swollen GI patch for fracture toughness measurement. L_c indicates the critical distance between the clamps at which the notch turns into a running crack. The measured fracture toughness of the GI patch is 758 J m^{-2}.

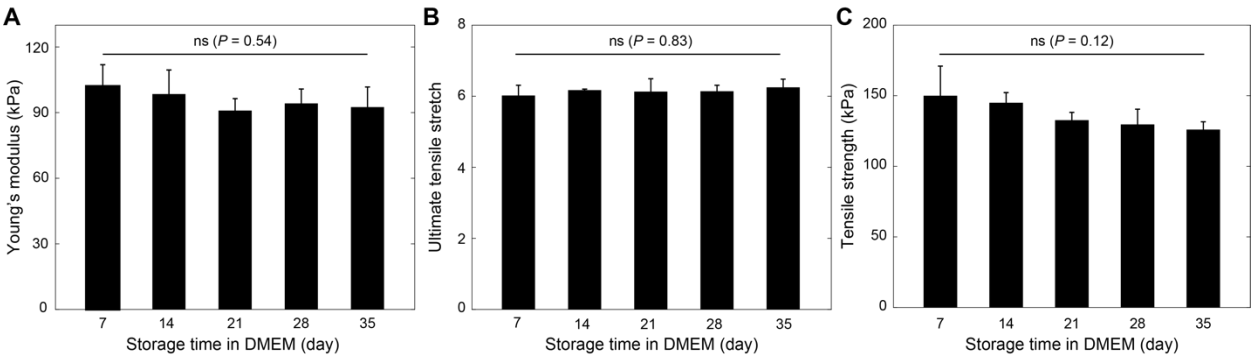

Fig. S7. Mechanical stability of the GI patch in physiological environment. (**A** to **C**) Young's modulus (A), ultimate tensile stretch (B), and tensile strength (C) of the GI patch stored in DMEM at 37 ℃ over time. DMEM, Dulbecco's Modified Eagle Medium. Values represent the means ± SD (n = 4). P values are determined by one-way ANOVA followed by the Bonferroni's multiple comparison test; ns, not significant.

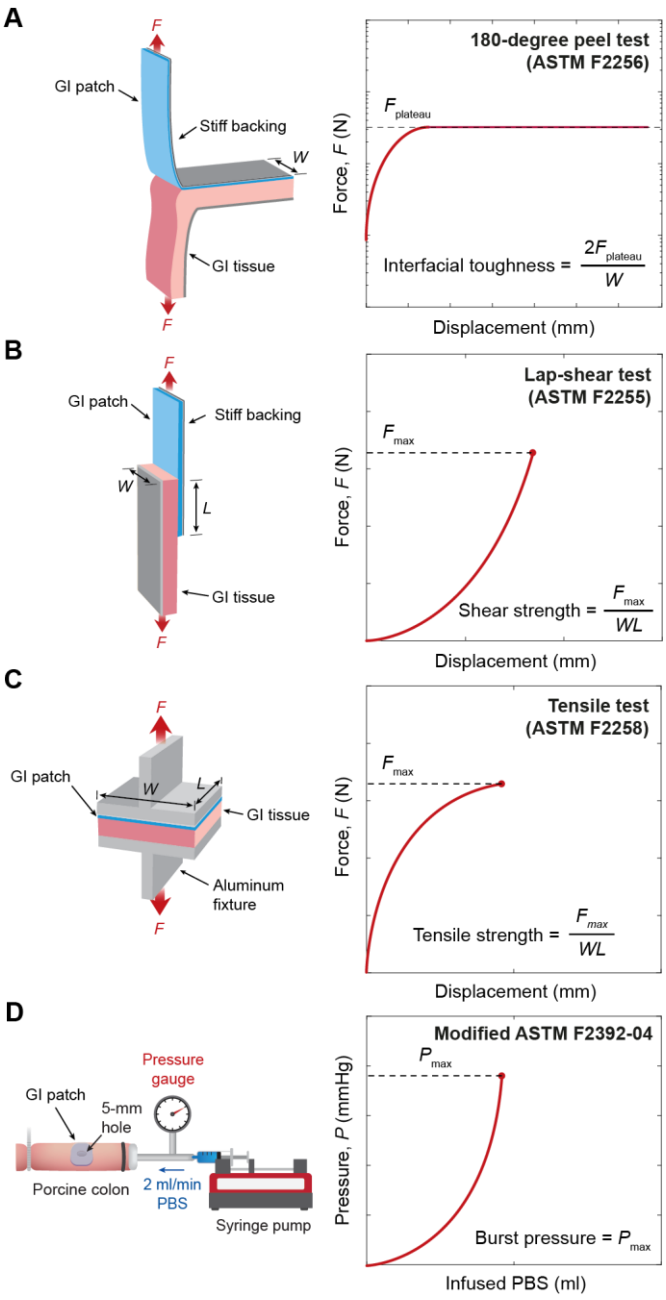

Fig. S8. Mechanical testing setups for evaluation of adhesion performance. (**A**) Schematic of testing setup for interfacial toughness measurements based on the standard 180-degree peel test (ASTM F2256). (**B**) Schematic of testing setup for shear strength measurements based on the standard lap-shear test (ASTM F2255). (**C**) Schematic of testing setup for wound closure strength measurements based on the standard tensile test (ASTM F2458-05). (**D**) Testing setup for burst pressure measurements (modified ASTM F2392-04). *F*, force; *W*, width; *L*, length; PBS, phosphate buffered saline.

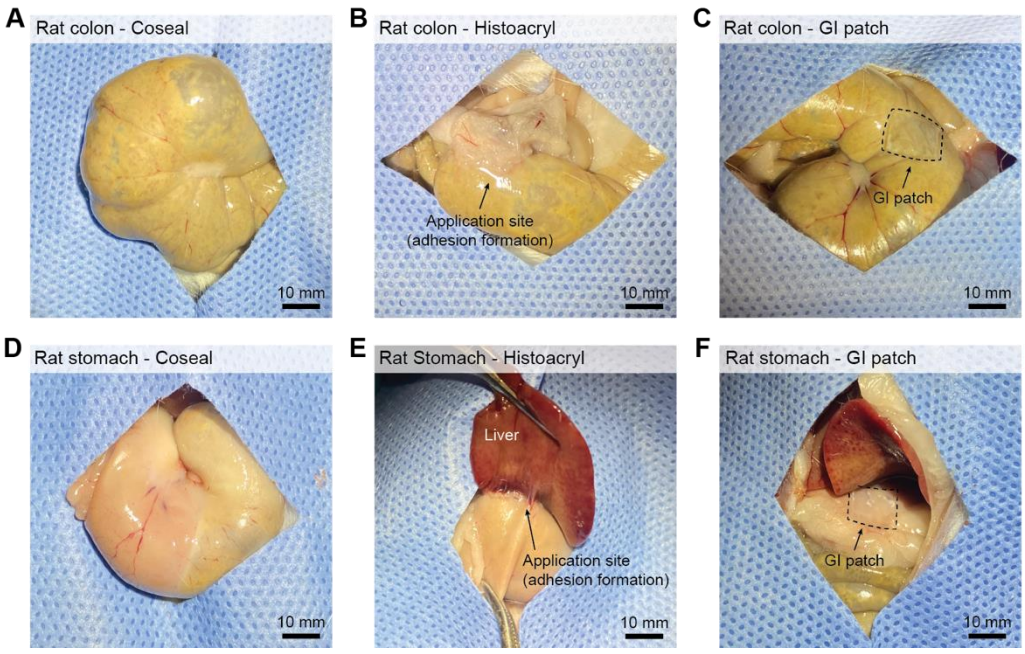

Fig. S9. Images of commercially available tissue adhesives and the GI patch implanted to rat GI organs. (**A** to **C**) Images of Coseal (A), Histoacryl (B), and the GI patch (C) at 4 weeks post-implantation to rat colon. (**D** to **F**) Images of Coseal (D), Histoacryl (E), and the GI patch (F) at 4 weeks post-implantation to rat stomach. n = 4 for each group. Scale bars, 10 mm.

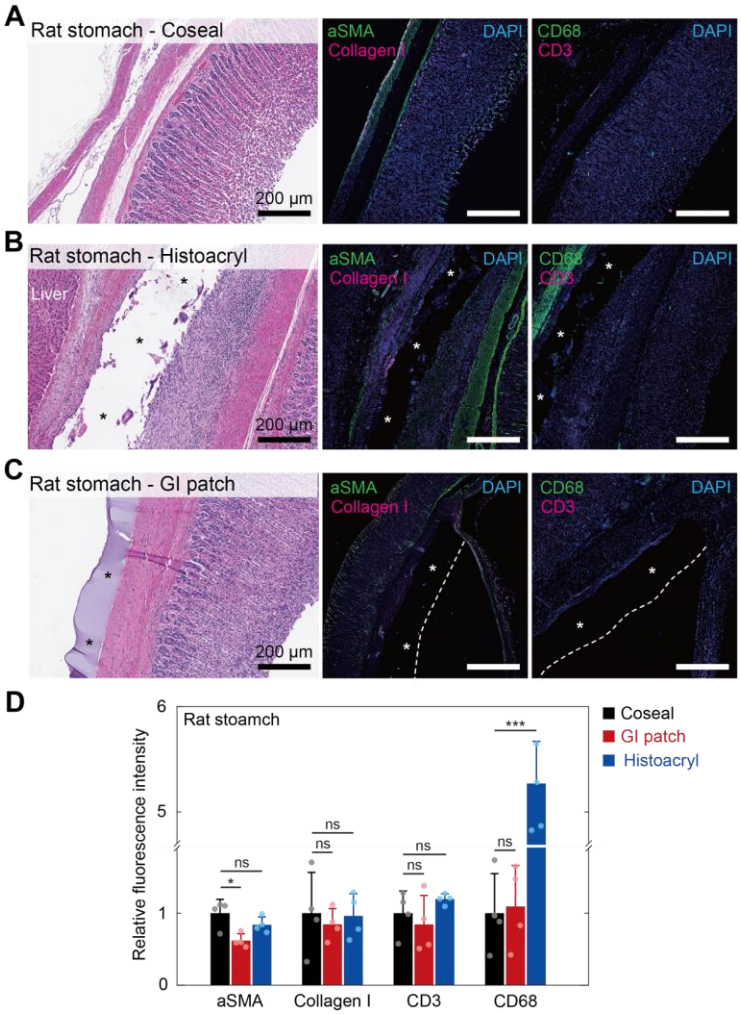

Fig. S10. In vivo biocompatibility of the GI patch in rat stomach model. (**A** to **C**) Representative histological images stained with HE (left) and immunofluorescence images (right) for Coseal (A), Histoacryl (B), and the GI patch (C) at 4 weeks post-implantation to rat stomach. In histological images, * represents the implanted Histoacryl (B) and GI patch (C). In immunofluorescence images, blue fluorescence corresponds to cell nuclei stained with DAPI; green fluorescence corresponds to the expression on fibroblast (aSMA) and macrophages (CD68); red fluorescence corresponds to the expression on Collagen I and T-cell (CD3); * represents the implanted Histoacryl (B) and GI patch (C); dotted line represents the edge of the implanted GI patch. (**D**) Normalized fluorescence intensity from the immunofluorescence images for aSMA, Collagen I, CD3, and CD68 at 4 weeks post-implantation of Coseal, Histoacryl, and the GI patch to rat stomach. Values in D represent the means ± SD (n = 4). P values are determined by two-sided t test; ns, not significant; * $P < 0.05$; *** $P \leq 0.001$. Scale bars, 200 μm (A to C).

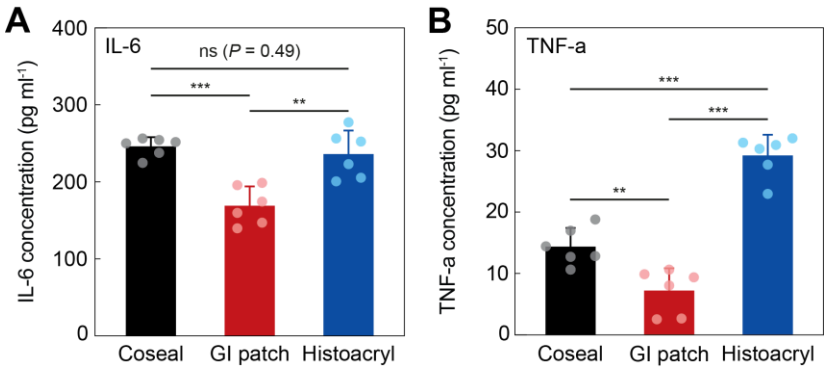

Fig. S11. ELISA assay. (**A** and **B**) IL-6 (A) and TNF-a (B) concentration of rat colon implanted with Coseal, Histoacryl, and the GI patch at 4 weeks post-implantation from ELISA assay. Values represent the means ± SD (n = 6). P values are determined by two-sided t test; ns, not significant; ** $P \leq 0.01$; *** $P \leq 0.001$.

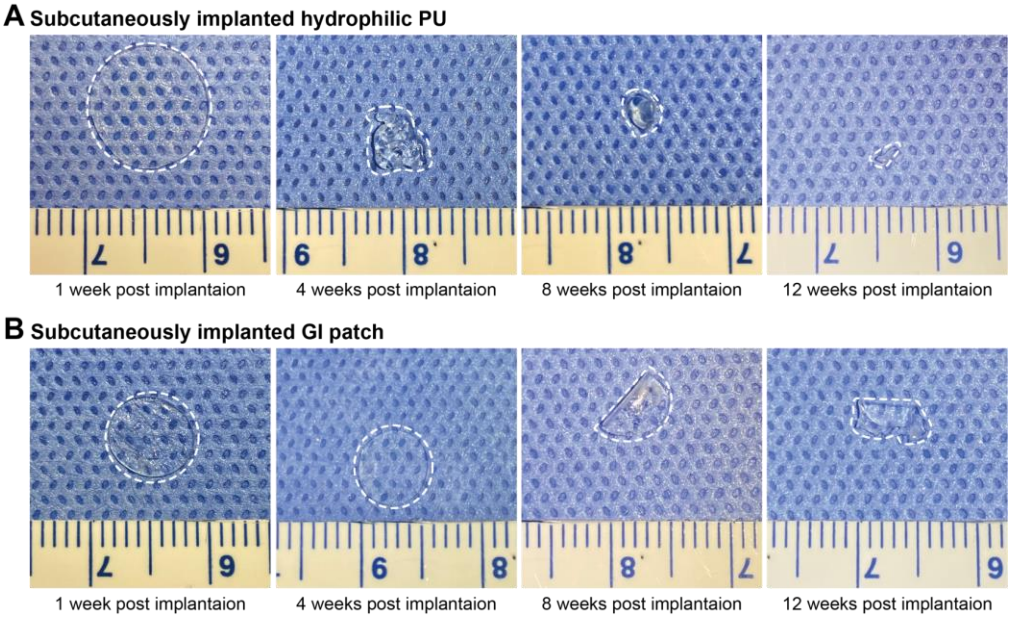

Fig. S12. In vivo degradation of hydrophilic PU and the GI patch in rat subcutaneous model. (**A** and **B**) Representative images of the subcutaneously implanted hydrophilic PU (A) and GI patch (B) at 1, 4, 8, and 12 weeks post-implantation. The samples were taken out of the subcutaneous space. Dotted lines represent the edge of the sample. $n = 4$ for each timepoint.

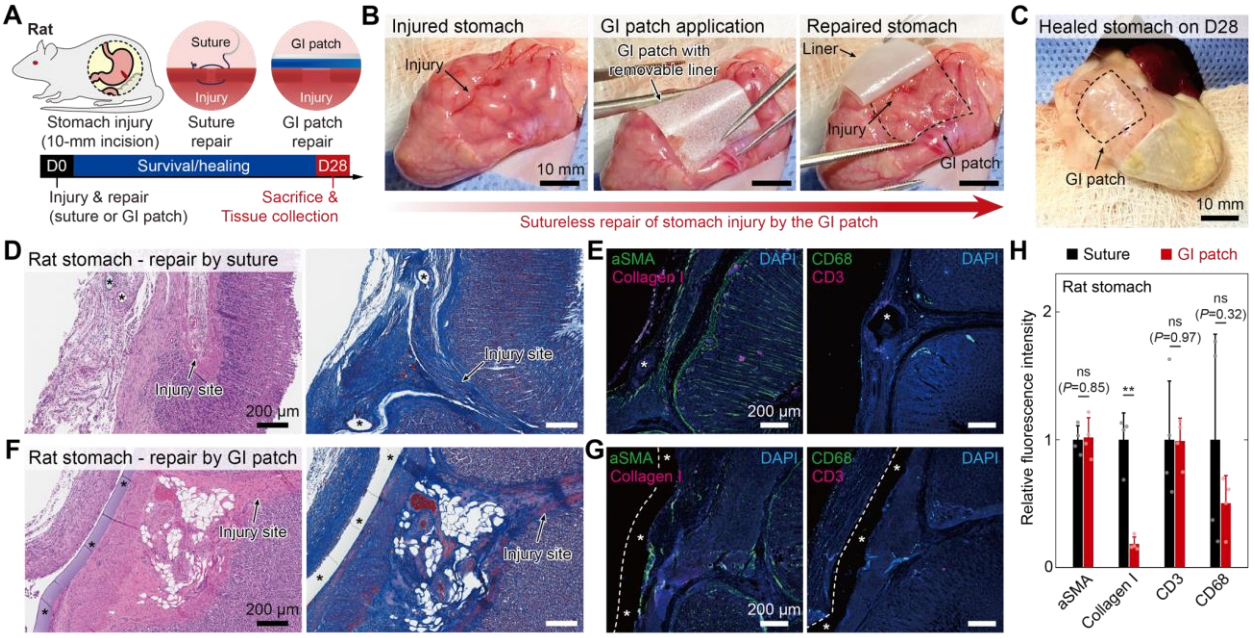

Fig. S13. Sutureless repair of GI defects in rat stomach model. (**A** and **B**) Schematic illustrations (A) and experimental images (B) for *in vivo* defect-repair studies of rat stomach by sutures and the GI patch. (**C**) Rat stomach 28 days (D28) after sutureless repair by the GI patch. (**D** to **G**) Representative histological images stained with HE and immunofluorescence images for rat stomach defect repaired by sutures (D and E) and the GI patch (F and G) after 28 days. In histological images, * represents the sutures (D) and GI patch (F). In immunofluorescence images, blue fluorescence corresponds to cell nuclei stained with DAPI; green fluorescence corresponds to the expression of fibroblast (aSMA) and macrophages (CD68); red fluorescence corresponds to the expression of Collagen I and T-cell (CD3); * represents the sutures (E) and GI patch (G); dotted line represents the edge of the GI patch. (**H**) Normalized fluorescence intensity from the immunofluorescence images for aSMA, Collagen I, CD3, and CD68 at 28 days after repair by sutures and the GI patch. Values in H represent the means ± SD (n = 4). P values are determined by two-sided t test; ns, not significant; ** $P \leq 0.01$. Scale bars, 10 mm (B and C); 200 μm (D to G).

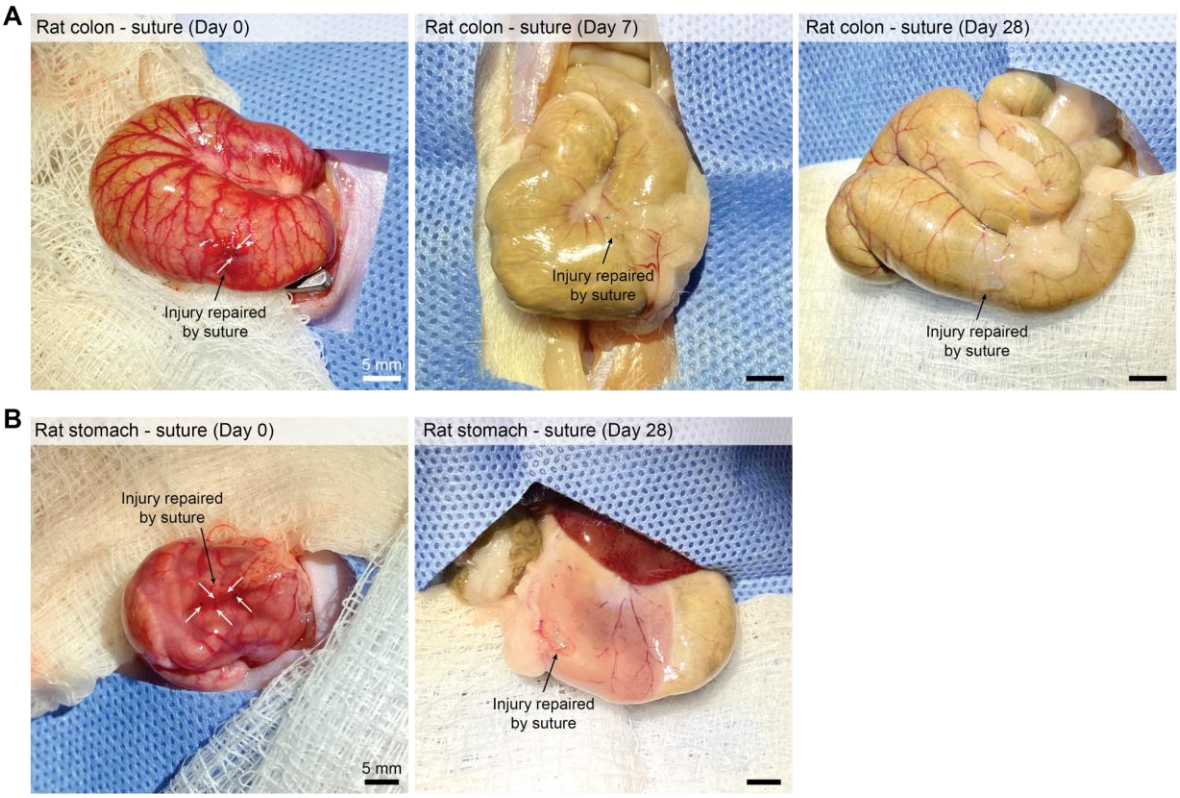

Fig. S14. Repair of GI defects by sutures in rat model. (**A** and **B**) Representative images of rat colon (A) and stomach (B) defects repaired by sutures immediately after sealing, after 7 days, and after 4 weeks. White arrows indicate the sites where tissue damage and bleeding were occurred through punctures by sutures. Scale bars, 5 mm.

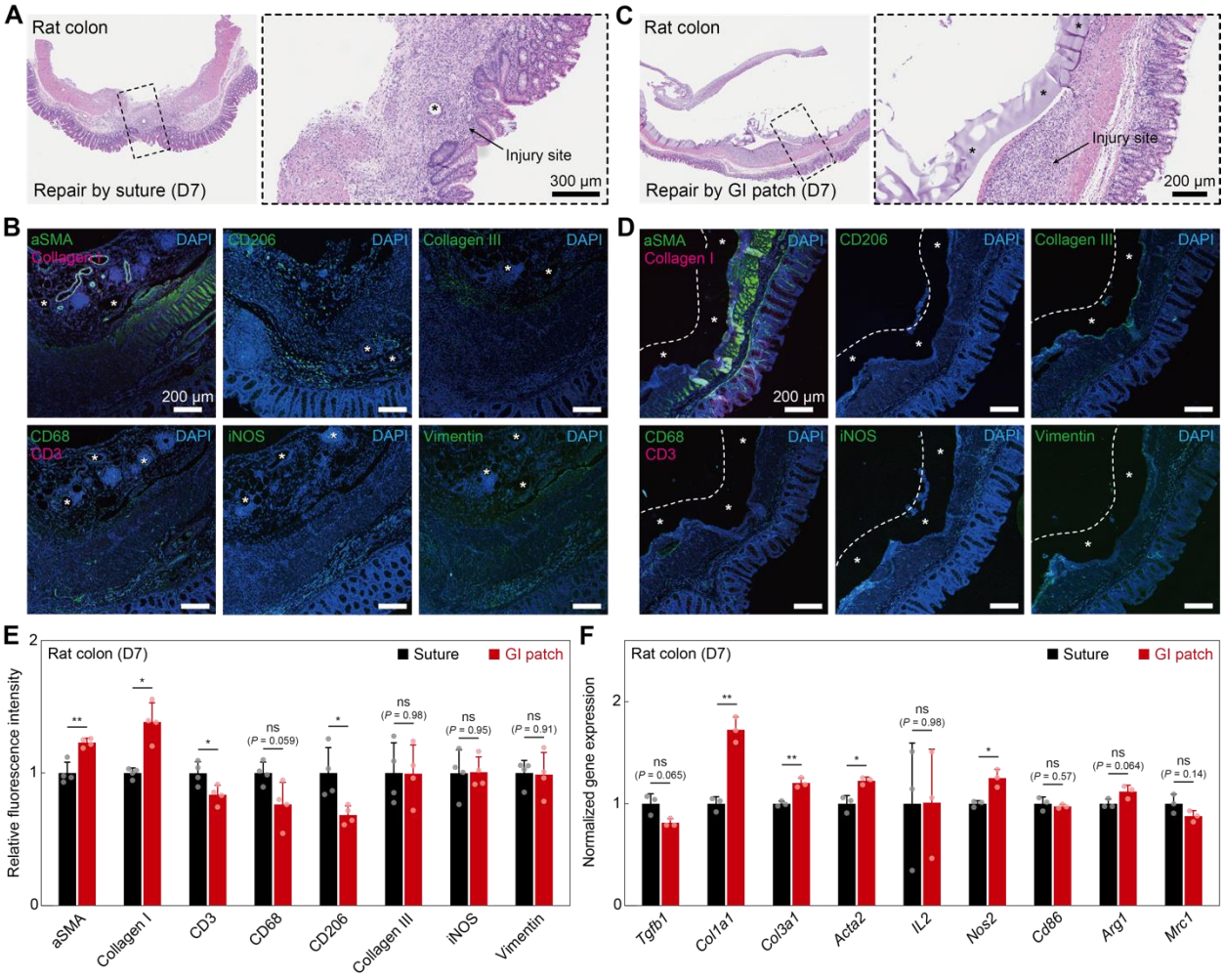

Fig. S15. Sutureless repair of GI defects in rat colon model. (**A** to **D**) Representative histological images stained with HE and immunofluorescence images for rat colon defect repaired by sutures (A and B) and the GI patch (C and D) after 7 days (D7). In histological images, * represents the sutures (A) and GI patch (C). In immunofluorescence images, blue fluorescence corresponds to cell nuclei stained with DAPI; green fluorescence corresponds to the expression of fibroblast (aSMA), Collagen III, Vimentin, pan macrophage (CD68), M1 type macrophage (iNOS), M2 type of macrophage (CD206); red fluorescence corresponds to the expression of Collagen I and T-cell (CD3); * represents the sutures (B) and GI patch (D); dotted line represents the edge of the implanted GI patch. (**E**) Normalized fluorescence intensity from the immunofluorescence images for aSMA, Collagen I, Collagen III, Vimentin, CD3, CD68, iNOS, CD206 at 7 days after repair by sutures and the GI patch. (**F**) Normalized gene expression of inflammation-related markers in rat colon at 7 days after repair by sutures and the GI patch. Values in E and F represent the means ± SD (n = 4 in E; n = 3 in F). P values are determined by two-sided t test; ns, not significant; * $P < 0.05$; ** $P \leq 0.01$; *** $P \leq 0.001$. Scale bars, 300 μm (A); 200 μm (B to D).

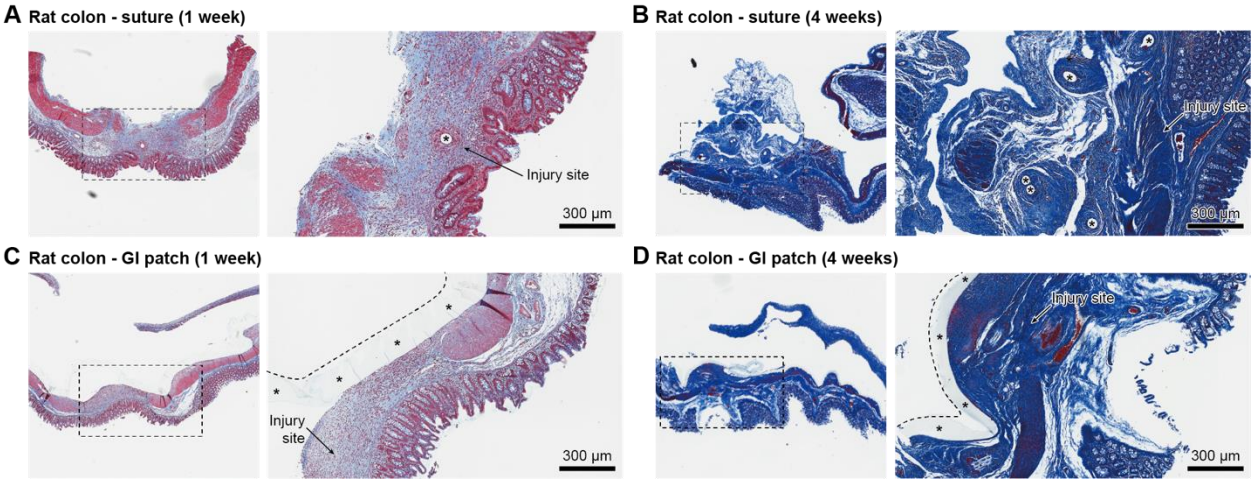

Fig. S16. Representative MT-stained histological images of rat colon. (**A** and **B**) Representative histological images stained with Masson's trichrome (MT) for rat colon defect repaired by sutures after 1 week (A) and 4 weeks (B). (**C** and **D**) Representative histological images stained with MT for rat colon defect repaired by the GI patch after 1 week (C) and 4 weeks (D). * represents sutures (A and B) and the GI patch (C and D); dotted line represents the edge of the implanted GI patch. $n = 4$ for each group. Scale bars, 300 μm.

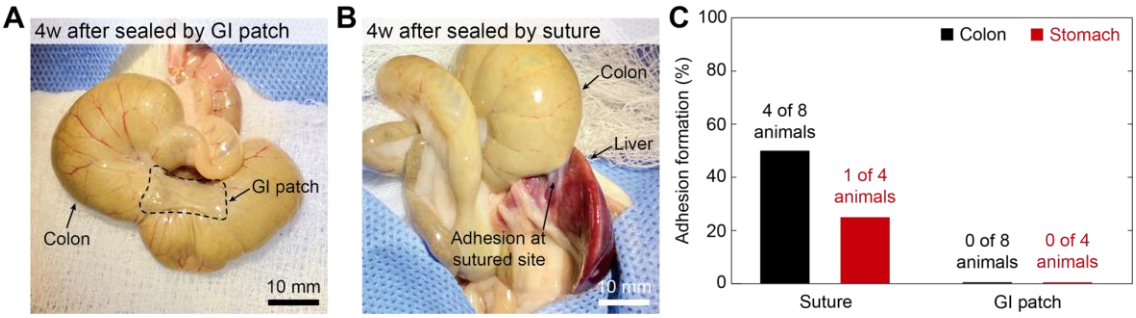

Fig. S17. Post-surgical adhesion of repaired rat GI organs. (**A** and **B**) Representative images of rat colon defect repaired by the GI patch (A) and sutures (B) after 4 weeks. Post-surgical adhesion to surrounding organs is observed at the sutured site (B). (**C**) Percentage of post-surgical adhesion formation for rat colon and stomach defects repaired by sutures and the GI patch. Scale bars, 100 mm.

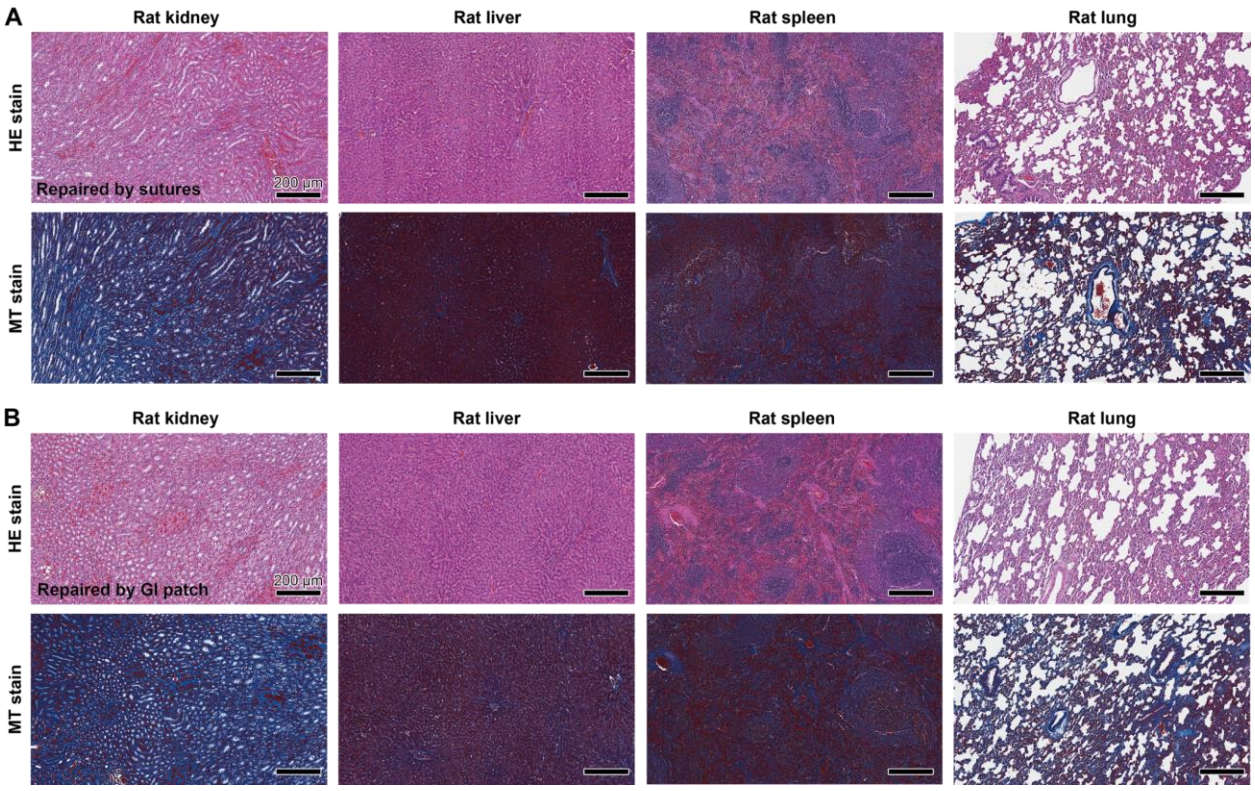

Fig. S18. Other organs in rat GI defect repair study. (**A**) Representative histological images stained with HE (top) and MT (bottom) for other organs in rat with colon defects repaired by sutures after 4 weeks. (**B**) Representative histological images stained with HE (top) and MT (bottom) for other organs in rat with colon defects repaired by the GI patch after 4 weeks. $n = 4$ for each group. Scale bars, 200 μm.

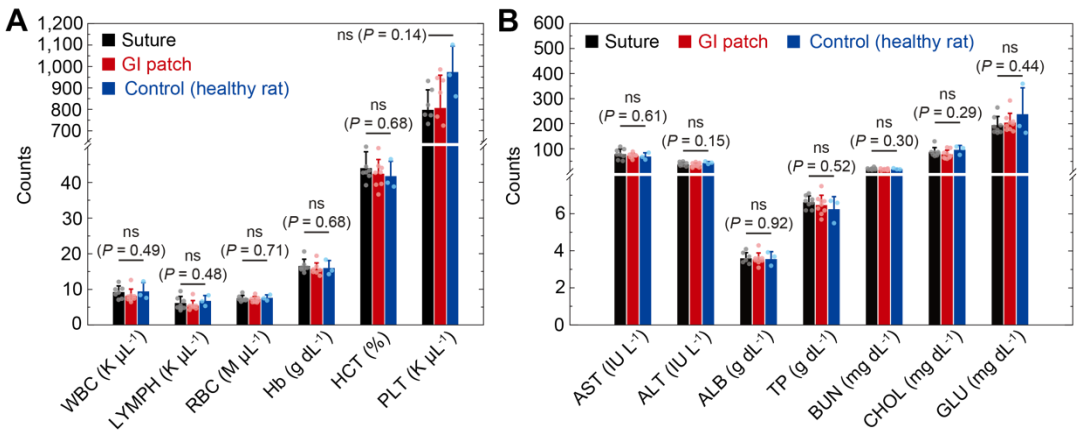

Fig. S19. Blood analysis for rat GI defect repair study. (**A**) Complete blood count (CBC) of control (healthy animal without surgery) and 4 weeks after repair of rat colon and stomach defects by sutures and the GI patch. WBC, white blood cell; LYMPH, lymphocyte; RBC, red blood cell; Hb, hemoglobin; HCT, hematocrit; PLT, platelet. (**B**) Blood chemistry of control (healthy animal without surgery) and 4 weeks after repair of rat colon and stomach defects by sutures and the GI patch. AST, aspartate transaminase; ALT, alanine transaminase; ALB, albumin; TP, total protein; BUN, blood urea nitrogen; CHOL, cholesterol; GLU, glucose. Values represent the means ± SD (n = 6). P values are determined by one-way ANOVA followed by the Bonferroni's multiple comparison test; ns, not significant.

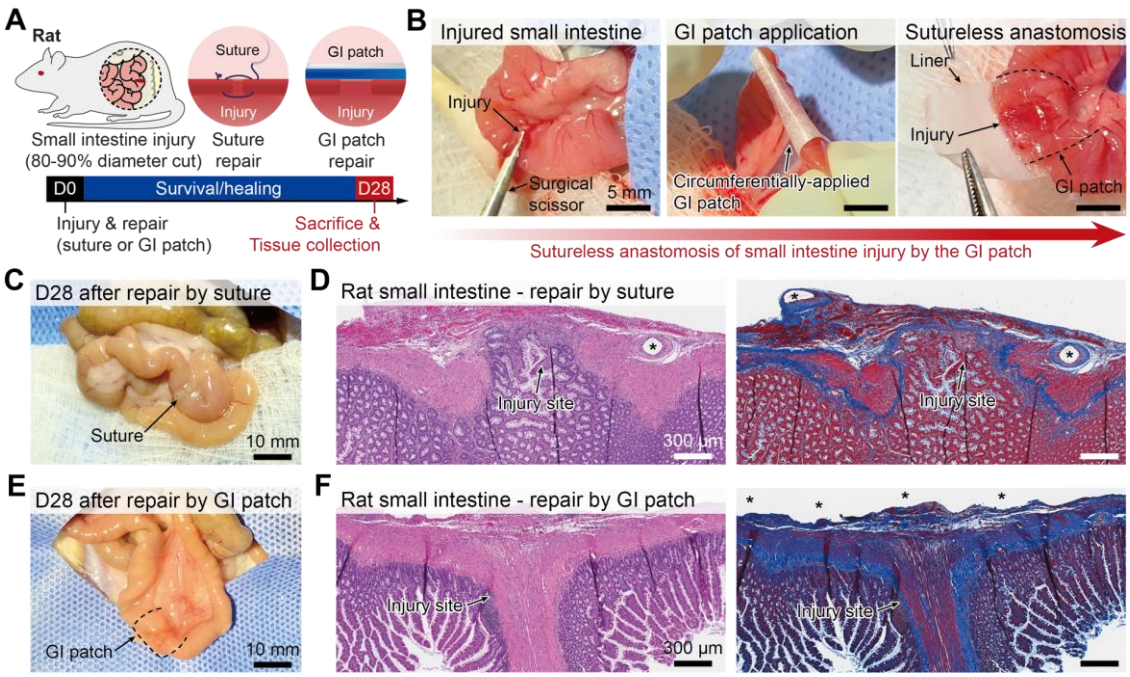

Fig. S20. Sutureless anastomosis of GI defects in rat small intestine model. (**A** and **B**) Schematic illustrations (A) and experimental images (B) for in vivo defect-repair studies of rat small intestine by sutures and the circumferentially-applied GI patch. (**C** and **E**) Photographs of rat small intestine 28 days (D28) after repair by sutures (C) and the GI patch (E). (**D** and **F**) Representative histological images stained with HE (left) and MT (right) for rat small intestine repaired by sutures (D) and the GI patch (F) after 28 days. * represents the sutures (D) and GI patch (F). *n* = 4 for each group. Scale bars, 5 mm (B); 10 mm (C and E); 300 μm (D and F).

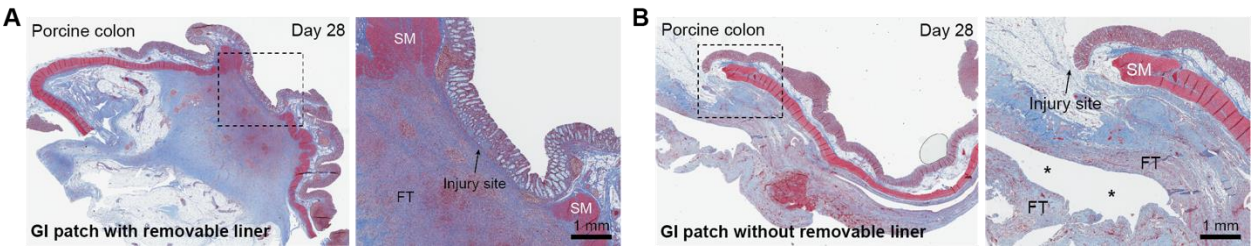

Fig. S21. Representative MT-stained histological images of porcine colon. (**A** and **B**) Representative histological images stained with MT for porcine colon defects treated with the GI patch with (A) and without (B) removable liner after 4 weeks. * represents the GI patch; SM, smooth muscle; FT, fibrous tissue. *n* = 2 for the GI patch with removable liner; *n* = 3 for the GI patch without removable liner. Scale bars, 1 mm.

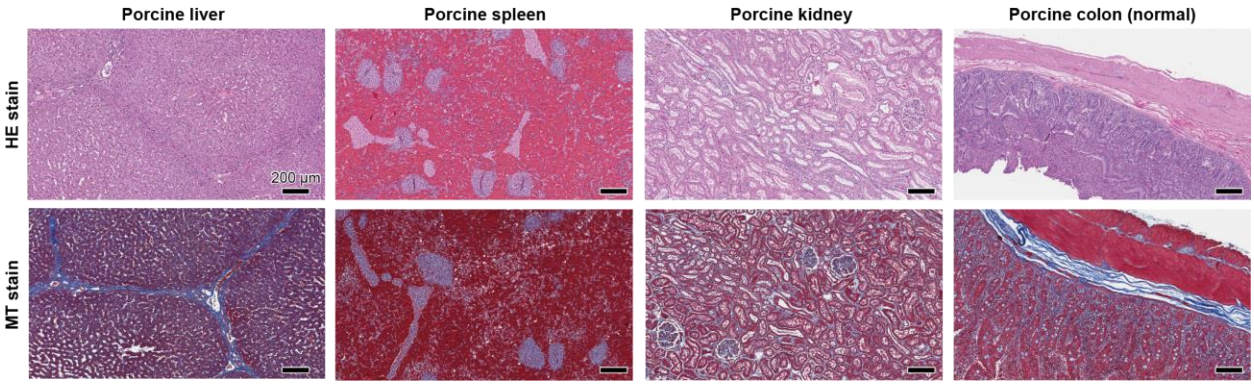

Fig. S22. Other organs in porcine GI defect-repair study. Representative histological images stained with HE (top) and MT (bottom) for other organs in pig with colon defects repaired by the GI patch without removable liner after 4 weeks (n = 3). Scale bars, 200 μm.

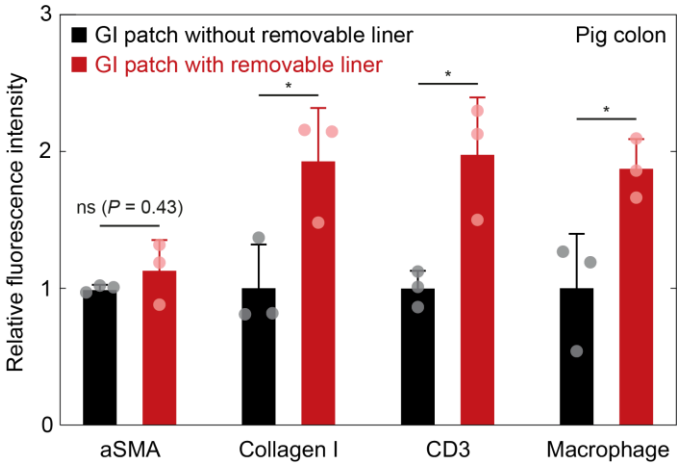

Fig. S23. Immunofluorescence analysis for porcine GI defect repair study. Normalized fluorescence intensity from the immunofluorescence images for aSMA, Collagen I, CD3, and Macrophage at 28 days after repair of porcine colon defects by the GI patch without and with removable liner. Values represent the means ± SD (n = 3). P values are determined by two-sided t test; ns, not significant; * $P < 0.05$.

Legends for Supplementary Data Files

Data file S1. Individual data and statistical analyses on the adhesion performance comparison between the fully swollen GI patch and commercial counterparts.

Data file S2. Individual data in Fig. 2A to F, H.

Data file S3. Individual data in Fig. 3A, H, I.

Data file S4. Individual data in Fig. 4D, F, G.

Data file S5. Individual data in Fig. 5H and I.

Legends for Supplementary Movies

Movie S1. Sutureless repair of a gastrointestinal defect in an ex vivo porcine colon by the GI patch.

Movie S2. Sutureless repair of a gastrointestinal defect in an ex vivo porcine stomach by the GI patch.

Movie S3. Sutureless repair of a gastrointestinal defect in an in vivo rat colon by the GI patch.

Movie S4. Sutureless repair of a gastrointestinal defect in an in vivo rat stomach by the GI patch.

Movie S5. Sutureless repair of gastrointestinal defects in an in vivo porcine colon by the GI patch.